

Aerosol Mass yields of selected Biogenic Volatile Organic Compounds – a theoretical study with near explicit gas-phase chemistry

Carlton Xavier¹, Anton Rusanen¹, Putian Zhou¹, Chen Dean¹, Lukas Pichelstofer¹, Pontus Roldin², Michael Boy¹

¹Institute for Atmospheric and Earth Systems Research (INAR), Physics, University of Helsinki

²Division of Nuclear Physics, Lund University, Box 118, SE-22100, Lund, Sweden

Correspondence : Carlton Xavier (carlton.xavier@helsinki.fi), Michael Boy (michael.boy@helsinki.fi)

Abstract

In this study we modeled secondary organic aerosols (SOA) mass loadings from the oxidation (by O₃, OH and NO₃) of five representative Biogenic Volatile Organic compounds (BVOCs): isoprene, endocyclic bond containing monoterpenes (α -pinene and limonene), exocyclic double bond compound (β -pinene) and a sesquiterpene (β -caryophyllene). The simulations were designed to replicate idealized smog chamber and oxidative flow reactors (OFR). The master chemical mechanism (MCM) together with the peroxy radical autoxidation mechanism (PRAM), were used to simulate the gas-phase chemistry. The aim of this study was to compare the potency of MCM and MCM+PRAM in predicting SOA formation. SOA yields were in good agreement with experimental values for chamber simulations when MCM+PRAM was applied, while a standalone MCM under-predicted the SOA yields. Compared to experimental yields, the OFR simulations using MCM+PRAM yields were in good agreement for BVOCs oxidized by both O₃ and OH. On the other hand, a standalone MCM under-predicted the SOA mass yields. SOA yields increased with decreasing temperatures and NO concentrations and vice-versa. This highlights the limitations posed when using fixed SOA yields in a majority of global and regional models. Few compounds that play a crucial role (>95% of mass load) in contributing to SOA mass increase (using MCM+PRAM) are identified. The results further emphasized that incorporating PRAM in conjunction with MCM does improve SOA mass yields estimation.

1. Introduction

Atmospheric secondary organic aerosols, formed from gas to particle phase conversion of the oxidation products of volatile organic compounds (VOC) significantly impact the organic aerosol mass loadings (Griffin, 1999; Kanakidou et al., 2005). However, the scale of SOA contribution to the aerosol particle mass is still subject to high uncertainties (Hao et al., 2011, Glasius and Goldstein, 2016). The elevated aerosol particle concentrations are shown to have inimical effects on health (Miller et al., 2007), and a varying degree of influence on the climate by forming cloud condensation nuclei (CCN), altering the cloud properties

31 and radiative balance (Rosenfeld et al., 2014; Schmale et al., 2018). Therefore, it is acutely necessary to
32 understand the role and contributions of SOA to the particle loading in the atmosphere. Biogenic VOCs from
33 forest are estimated to contribute to about 90% of VOCs emissions globally (Guenther et al., 1995, 1999 and
34 2000). The most important BVOCs for SOA formation are isoprene (C_5H_8), monoterpenes ($C_{10}H_{16}$) and
35 sesquiterpenes ($C_{15}H_{24}$). These compounds are all alkenes containing at least one carbon-carbon double bond,
36 enabling them to undergo oxidation by the dominant atmospheric oxidants: the hydroxyl radical (OH), ozone
37 (O_3) and the nitrate radical (NO_3). For some of the terpenes, initial oxidation steps can lead to formation of
38 highly oxygenated organic molecules (HOM). These HOMs generally have low volatilities and can condense
39 nearly irreversibly, thereby producing SOA (Ehn et al., 2014). HOMs, detected in both the ambient
40 atmosphere and chamber experiments (Ehn et al., 2012) are formed by autoxidation (Berndt et al., 2016;
41 Crouse and Nielsen, 2013) wherein peroxy radicals (RO_2) undergo subsequent intramolecular H-shifts
42 accompanied by rapid reactions with O_2 . Autoxidation hence results in compounds containing multiple
43 functional groups such as hydroxyls, peroxides and carbonyls (Bianchi et al., 2017, Bianchi et al., 2019).

44 A majority of chamber and flow-tube experiments have focused on HOM formation from the
45 oxidation of various VOCs and their contribution to SOA mass loadings (Ehn et al., 2014; Kristensen et al.,
46 2017). Oxidation of isoprene (Liu et al., 2016), endocyclic monoterpenes containing reactive double bonds
47 such as α -pinene and limonene (Zhao et al., 2015), or exocyclic double bond containing compounds such as
48 β -pinene (Jokinen et al., 2015) and sesquiterpenes such as β -caryophyllene (Chen et al., 2012) have been
49 investigated. The SOA forming potential of various BVOCs depends on the isomeric structures (Friedman
50 and Farmer, 2018; Keywood et al., 2004). Ozonolysis of compounds containing reactive endocyclic bonds
51 such as α -pinene produce higher SOA mass yields of 41% in comparison to those with exocyclic bonds (β -
52 pinene), which produce mass yields of 17% (Lee et al., 2006a). One explanation for this dependence on the
53 isomeric structure is attributed to the formation of HOMs (Ehn et al., 2014). Another important factor
54 influencing HOM formation is the initial oxidant, as pointed out by Zhao and co-workers (2015). They
55 showed that the SOA formation by OH oxidation of α -pinene and limonene were lower when compared to
56 their SOA formed by ozonolysis. Further they measured lower H/C ratio for SOA produced by monoterpene
57 ozonolysis (experiments were carried out in dark with CO as OH scavenger), in comparison to OH oxidation
58 of α -pinene and limonene, while O/C ratio were similar for both oxidation cases. This was attributed to the
59 formation of RO_2 radicals (monoterpenes + O_3) which undergo internal hydrogen shifts and subsequently react
60 with another RO_2 radical, to form compounds containing carbonyl groups while losing hydrogen atoms in the
61 process. A similar analysis was conducted by Draper et al. (2015), who showed that an increase in NO_2
62 concentration reduced α -pinene ozonolysis SOA mass yields, while no appreciable reduction in mass yields

63 are reported for β -pinene and Δ^3 -carene ozonolysis. On the other hand, the mass yields from limonene
64 ozonolysis increased with increasing NO_2 concentrations (Draper et al., 2015). This disparity in mass yields
65 for different BVOCs in the presence of NO_2 is possibly caused by the formation of high molecular weight
66 oligomers (or lack of in case of α -pinene) through oxidation with NO_3 that contribute to SOA mass loadings
67 (Draper et al., 2015).

68 Due to computational limitations, many regional and canopy scale atmospheric chemistry models
69 generally use isoprene and/or a representative monoterpene (generally α -pinene), to model SOA yields
70 (Friedman and Farmer, 2018). The SOA yields of different monoterpenes vary with structure, NO_x and
71 temperature (Friedman and Farmer, 2018; Kristensen et al., 2017; Presto et al., 2005). This poses a limitation
72 on using representative monoterpene fixed SOA yields in many of the global models and increases
73 uncertainties in predicting cloud condensation nuclei concentrations, cloud droplet number concentrations and
74 radiative balance due to aerosol loadings.

75 This work aims to investigate the SOA mass loading from the oxidation products of BVOCs with the
76 atmospheric oxidants OH, O_3 and NO_3 with a specific focus on the BVOCs isoprene, α -pinene, β -pinene,
77 limonene and β -caryophyllene. Further we study the effect of varying temperature (258.15 K – 313.15 K) and
78 NO concentrations (0 - 5 ppb) on α -pinene oxidation mass yields. We use the master chemical mechanism
79 (MCMv3.3.1) (Jenkin et al., 1997, 2012 and 2015; Saunders et al., 2003), a near explicit gas-phase chemical
80 mechanism together with peroxy radical autoxidation mechanism (PRAM, Roldin et al., 2019) (PRAM +
81 MCM). The aim is to understand the importance and contribution of peroxy radical autoxidation products to
82 the SOA mass yields from terpenes.

83

84 2. Model description

85 2.1 Malte Box

86 MALTE (Model to predict new Aerosol formation in Lower TropospherE) is a one-dimensional
87 model consisting of modules calculating boundary layer meteorology, emissions of BVOCs, gas-phase
88 chemistry and aerosol dynamics with the aim to simulate particle distribution and growth in the lower
89 troposphere (Boy et al., 2006). In this study, a zero-dimensional version, MALTE-Box is applied to simulate
90 an ideal chamber and flow-tube environment (i.e. no wall losses effects are considered in this study). For the
91 simulations performed in this study the emission module was switched off while only employing the gas-
92 phase chemistry and aerosol dynamics module.

93 Kinetic preprocessor (KPP) is used to generate a system of coupled differential equations to solve the
94 gas-phase chemistry schemes (Damian et al., 2002). The peroxy radical autoxidation mechanism (PRAM),
95 (Roldin et al., 2019, Qi et al., 2018, Öström et al., 2017), formulated based on the oxidation of monoterpenes
96 as described by Ehn et al. (2014) was incorporated alongside MCMv3.3.1. PRAM explicitly describes the
97 formation and evolution of peroxy radicals (RO_2) from the ozonolysis and OH oxidation of monoterpenes,
98 driven by subsequent H-shifts and O_2 additions. The current version of PRAM based on experimental and
99 theoretical studies, considers HOM autoxidation for a fraction of the peroxy radicals formed during the
100 ozonolysis of α -pinene and limonene and OH oxidation of α -pinene, β -pinene and limonene. This is achieved
101 by assigning species specific molar yields for the formation of first RO_2 , which subsequently initiates the
102 autoxidation chain (Roldin et al., 2019). Currently, in PRAM a maximum first generation RO_2 yield of 9% for
103 α -pinene ozonolysis, 21.9 % for limonene ozonolysis, 2.5 % for α -pinene+OH, and 1% for both
104 limonene+OH and β -pinene+OH first generation products are allowed to initiate autoxidation (Roldin et al.,
105 2019). For β -pinene ozonolysis the molar yield of RO_2 is minor (<0.1 %) (Roldin et al., 2019, Ehn et al. 2014)
106 and hence not considered in this work. The above mentioned RO_2 molar yields used in this work are close to
107 the experimental values obtained in both smog chamber and flow tube experiments. Ehn et al. (2014)
108 measured an RO_2 yield of ~7% for α -pinene ozonolysis and ~17% for limonene ozonolysis, whereas Jokinen
109 et al. (2015) measured 0.58 % and 0.93 % for OH oxidation of β -pinene and limonene respectively. The
110 autoxidation is terminated by bimolecular reactions, wherein the RO_2 formed reacts with NO, HO_2 or other
111 peroxy radicals, thereby forming alkoxy radicals, closed shell monomers or dimers (Roldin et al., 2019). The
112 PRAM considers temperature dependent autoxidation reaction rates, which is important when investigating
113 the SOA mass yields at varying temperatures (Table 1e). The temperature dependence in PRAM is based on
114 quantum chemical calculations wherein the autoxidation rates correspond to an activation energy of 24
115 kcal/mol. The activation energies vary for autoxidation of different RO_2 from α -pinene ozonolysis between 22
116 and 29 kcal/mol (Rissanen et al., 2015), leading to varying autoxidation rates at different temperatures
117 (Roldin et al., 2019). It should be noted that the temperature dependence in PRAM is a first of its kind but
118 needs further evaluation using recent measurements of HOM formation at different temperatures (e.g.
119 Quéléver et al., 2019).

120 The aerosol dynamics are simulated using the University of Helsinki Multicomponent Aerosol model
121 (UHMA) originally from Korhonen et al. (2004). The model has undergone significant development since
122 then to allow simulation with all the compounds from MCM. It now supports an unlimited number of
123 condensing vapors and solves condensation using the analytical predictor of condensation method from
124 Jacobson (1997). The condensation algorithm considers both, the Kelvin effect and Raoult's law. The

125 processes included in the model are nucleation, condensation, evaporation, coagulation and deposition. The
126 discretization of the size distribution and the time evolution is modeled with the moving section approach,
127 with optional redistribution to a fixed grid. In this work, the redistribution is active to make the coagulation
128 more accurate, since it requires that grid points are available near the size of the coagulated particles. In this
129 study nucleation and deposition are not active, and hence are not considered. A total of 100 size bins ranging
130 from 1nm to 20 μm with the fixed grid was applied for this study.

131 A group contribution method based on Nannoolal et al. (2008) using the UManSysProp online system
132 (Topping et al., 2016) was used to estimate the pure liquid saturation vapor pressures (p_0) of the organic
133 compounds in MCMv3.3.1. For the PRAM species, p_0 were estimated using the functional group method
134 SIMPOL (Pankow and Asher, 2008; see Roldin et al., 2019 for details). Temperature was used as an input to
135 estimate p_0 for both the group contribution methods.

136 2.2 Simulations

137 The simulations performed in this study are aimed to closely resemble an idealized smog chamber
138 (batch mode setup) and an Oxidative Flow Reactor (OFR) without interactions between the gas phase and the
139 system walls. For the chamber runs, the VOC and oxidants were introduced at the beginning (time, $t=0$ sec),
140 set to certain concentrations (Table 1a) and then allowed to react. Both chamber and OFR simulations are
141 performed using ammonium sulfate seed particles which are introduced at time $t=0$. The condensation sink
142 (CS) was inferred from the size distribution of seed particles used in the model. The CS for the chamber and
143 OFR simulations was set to 0.00067 s^{-1} and 0.067 s^{-1} respectively. SOA mass yields obtained using an OFR
144 are sensitive to short residence time used, hence the seed particle surface area should be chosen in order to
145 overcome the mass yield underestimation (Ahlberg et al., 2019). CS sensitivity runs (Supplement Figure S1)
146 were performed for α -pinene- O_3 to determine the CS for which there are no appreciable change in mass yields
147 with increasing particle surface.

148 The simulation for the chamber setup is run for a maximum time of 24 hours and ends when either of
149 the 2 criteria are satisfied: (1) the simulation time reaches the 24-hour mark or (2) 90 % of the initial
150 precursor VOC has reacted away. In the latter case the simulation is continued for an additional 2 hours to
151 ensure enough time for the vapors to condense onto the seed particles. By contrast, the OFR runs were
152 simulated for a maximum residence time of 100 seconds, ensuring all initial precursor vapors were oxidized.
153 Seed particles were also added in the OFR simulations. The oxidant concentrations used for the OFR
154 simulations (Table 1b) are significantly higher in comparison to the simulated chamber runs (~ 2 orders of
155 magnitude larger). The time step for the chamber and flow-tube simulations are set to $t=10\text{ s}$ and $t=0.1\text{ s}$

156 respectively. The runs performed were oxidant specific (i.e. VOCs would be oxidized by only one specific
 157 oxidant at any given time). For the O₃ specific simulations no OH could form in both, OFR and chamber
 158 setups, thus enabling oxidation of O₃ to be the only pathway.

159 The simulations were performed at atmospheric relevant NO_x (NO_x = NO +NO₂) concentrations,
 160 corresponding to [NO]=0.5 ppb and [NO₂] = 2.0 ppb conditions with the relative humidity (RH) set to 60 %
 161 and temperature to 293.15 K. The RH value considered in this study is based on previous published
 162 experimental studies performed at ~60 % in both smog chamber (Bruns et al., 2015a; Ehn et al., 2014;
 163 Stirnweis et al., 2017) and OFR (Ahlberg et al. et al., 2018). α-pinene ozonolysis runs were performed at four
 164 different temperatures: 258.15 K, 278.15 K, 303.15K and 313.15 K, respectively (Table 1c) . SOA mass
 165 yields are expected to increase with decreasing temperature (Saathoff and Naumann, 2009). A similar
 166 temperature dependence was observed by Kristensen et al. (2017) who observed SOA mass yield from α-
 167 pinene ozonolysis at ~ 40 % and ~20 % at 258 K and 293 K respectively. Analogous to analyzing the effect of
 168 varying temperature on SOA yields, we study the variation in α-pinene ozonolysis SOA mass yields by
 169 varying the NO_x concentrations (Table 1c) . SOA yields for α-pinene ozonolysis at high NO_x conditions
 170 should be suppressed (Ng and Chhabra, 2007), which could be due to the production of relatively, volatile
 171 organic nitrates under high NO_x conditions as compared to less volatile products during low NO_x conditions
 172 (Presto et al., 2005).

173 Furthermore, two different chemistry schemes were applied for the simulations. One scheme consisted
 174 of only the MCM chemistry mechanism and the second included the MCM+PRAM chemistry mechanism.
 175 Table 1a shows the concentrations of different BVOCs and Table 1b shows the oxidants concentrations used
 176 for the simulations.

177 **Table 1a.** Concentrations of different BVOCs

| α-pinene (ppb) | β-pinene (ppb) | Isoprene (ppb) | Limonene (ppb) | B-caryophyllene (ppb) |
|---|---|----------------------------|---------------------------------|--------------------------|
| 0.5, 1.0, 5.0, 50.0, 100.0, 200.0 | 0.5, 1.0, 5.0, 50.0, 100.0, 200.0 | 5.0, 50.0, 100.0, 200.0 | 1.0, 5.0, 50.0, 100.0, 200.0 | 0.5, 1.0, 2.0, 5.0, 10.0 |

178

179 **Table 1b.** Concentrations of different oxidants for chamber and flow-tube runs

| | | |
|---|--|--|
| OH (* 10 ⁶ #/cm ³) - chamber | O ₃ (* 10 ¹¹ #/cm ³) - chamber | NO ₃ (* 10 ⁷ #/cm ³) - chamber |
| OH (* 10 ⁸ #/cm ³) - OFR | O ₃ (* 10 ¹³ #/cm ³) - OFR | NO ₃ (* 10 ⁹ #/cm ³) - OFR |

| | | |
|----------------------------|----------------------------|----------------------------|
| 2.0, 5.0 ,10.0, 50.0,100.0 | 1.0, 5.0 ,10.0, 50.0,100.0 | 1.0, 5.0 ,10.0, 50.0,100.0 |
|----------------------------|----------------------------|----------------------------|

180

181 **Table 1c.** NO concentrations and temperatures used for α -pinene ozonolysis

| | |
|------------------------|--|
| NO (ppb) | 0.5 (default), 0, 0.2, 1, 2, 5 |
| Temperature (K) | 293.15 (default), 258.15, 278.15, 303.15, 313.15 |

182

183 **2.3 Mass Yields**

184 The SOA mass yields (Y) are determined by calculating the ratio of the amount of SOA or mass
185 concentration of organic aerosol formed (C_{OA}) to the amount of VOC (ΔVOC) reacted:

186

$$Y = \frac{C_{OA}}{\Delta VOC} \quad (1)$$

187

188 A volatility basis set is fit to the data to obtain the volatility distribution. In this study equilibrium
189 partitioning was only assumed for deriving the volatility distribution based on the model simulations.

189 Following Donahue et al. (2006), the SOA is assumed to be in equilibrium with the gas-phase and using the

190 effective saturation concentration C_i^* spaced logarithmically. The individual product partitioning to the

191 particle phase can be estimated using

192

$$E_i = \left(1 + \frac{C_i^*}{C_{OA}} \right)^{-1} \quad (2)$$

193

194 Where E_i is the fraction of species in the condensed particle phase. The above equation determines the
195 fraction of species in the particle phase as well as in the gas phase. For example, if we assume $C_{OA} = 10 \mu\text{g m}^{-3}$

196 a species with $C^* = 10 \mu\text{g m}^{-3}$ will partition 50 % to condensed phase and the rest 50% will reside in the gas

197 phase. The fidelity of this equilibrium partitioning enables the parameterization of product vapors in volatility

198 C^* bins that are near the C_{OA} concentrations (Henry et al., 2012).

198 **3. Results and Discussion**

199

199 SOA mass yields were simulated for the oxidation of various biogenic volatile organic compounds

200 (isoprene, α -pinene, limonene and β -caryophyllene, β -pinene) by dominant atmospheric oxidants OH, O_3 and

201 NO_3 . The following section examines the comparison between the yields derived using MCM+PRAM and a

202 standalone MCM for chamber and flow-tube experiments.

203

204 3.1 BVOCs – O₃ chamber and flow-tube simulations

205 In Fig. 1 panel A indicates the SOA mass yields derived on applying a coupled MCM+PRAM mechanism to
206 ozonolysis of α -pinene and limonene (PRAM is only available for ozonolysis of α -pinene and limonene) and
207 the lower panel B shows ratio of yields obtained by MCM and coupled MCM+PRAM.

208 The abscissa, depicted on a log scale, considers the entire range of SOA mass loadings from 1-~~1150~~
209 **800** $\mu\text{g m}^{-3}$. Each data point is representative of simulated SOA mass yields resulting from variable BVOC
210 loading. The resulting mass yields for α -pinene in the range shown in Table 2a. are consistent with the yields
211 found in various smog chamber experiments. The mass yields derived using MCM+PRAM for α -pinene
212 ozonolysis are in good agreement with the experimental yields measured for similar mass loadings by
213 Kristensen et al. (2017) and Pathak et al. (2007). The standalone MCM, on the other hand, severely under-
214 predicts the mass yields for α -pinene ozonolysis. The MCM+PRAM also shows better agreement with
215 experiments when estimating the lower range mass yields for SOA mass loadings of $< 15 \mu\text{g m}^{-3}$. This is
216 supported by the values obtained by Shilling et al. (2008), where the authors measured a 0.09 yield from α -
217 pinene ozonolysis for SOA mass loading of $10.6 \mu\text{g m}^{-3}$. Limonene ozonolysis mass yields using
218 MCM+PRAM in comparison to standalone MCM, are much closer to the values given by Waring (2016).

219 The formation of HOM from β -pinene ozonolysis is low (Ehn et al., 2014; Jokinen et al., 2015) and
220 hence not considered in PRAM. The peroxy radical autoxidation mechanism for β -caryophyllene ozonolysis
221 has not yet been developed and therefore, not considered in PRAM. When comparing the measured mass
222 yield values for β -caryophyllene (Chen et al. 2012) and β -pinene ozonolysis (Griffin (1999) and Pathak et al.
223 (2008)) to the modeled values using the MCM scheme, it is evident that the MCM scheme drastically under-
224 predicts the SOA mass yields (Fig. 2).

225 Today oxidation flow reactor (OFR) experiments are complementing the traditional batch mode smog
226 chamber experiments. The OFR generally exhibits lower mass yields compared to the smog chamber
227 experiments at ranges of equivalent oxidant exposure (Lambe et al., 2015). We modeled flow-tube simulation
228 after the potential aerosol mass (PAM) OFR, where the residence time is in the order of a few to several
229 minutes (Lambe et al., 2011). The model simulations are performed with a maximum residence time of 100
230 seconds with O₃ exposures ranging from $1.0 \times 10^{15} - 1.0 \times 10^{17}$ molecules $\text{cm}^{-3} \text{s}$ (residence time * [O₃]).
231 Kang and Root (2007) measured a ~~value~~ **yield** of 0.2 for ozonolysis of α -pinene for an initial precursor VOC
232 concentration of 100 ppbv, while we obtain ~ 0.25 (MCM+PRAM) for the similar initial precursor
233 concentrations. The OFR yields for β -pinene (MCM-only) are significantly lower (0.02) than the values

234 measured by Kang and Root (2007) wherein they measured a yield of 0.49 for similar initial precursor
 235 concentrations. Addition of seed particles promotes condensation, leading to increased SOA yields (Lambe et
 236 al., 2015) which was confirmed by Ahlberg et al, (2019). Kang and Root (2007) found that using seed
 237 particles, the yield from α -pinene ozonolysis increased by a factor of ~ 1.4 which can explain our yields for α -
 238 pinene ozonolysis simulations. The mass spectra plot (Figure S2) shows that PRAM contributes the majority
 239 of dimers to the particle phase, while MCM dominate monomer contribution. Another interesting facet of
 240 Figure S2 are the different condensing compounds in both OFR and chamber simulations. The higher absolute
 241 RO_2 concentrations in the OFR simulations explain the lower concentration of HOM monomers and dimers
 242 relative to the chamber simulations, i.e. the high RO_2 concentrations in the OFR cause termination of the
 243 peroxy radical autoxidation chain before the RO_2 become highly oxygenated, thereby influencing SOA yields.
 244 Hence, this should be taken into account when using yields from OFR as inputs to regional and global
 245 models.

Table 2a. Mass yields for BVOCs ozonolysis at 293 K for different range of mass loadings using a chamber[†]
 setup. The values in parenthesis in the column ‘Experimental yields’ indicates the corresponding experimental
 mass loadings in unit of $\mu\text{g m}^{-3}$.

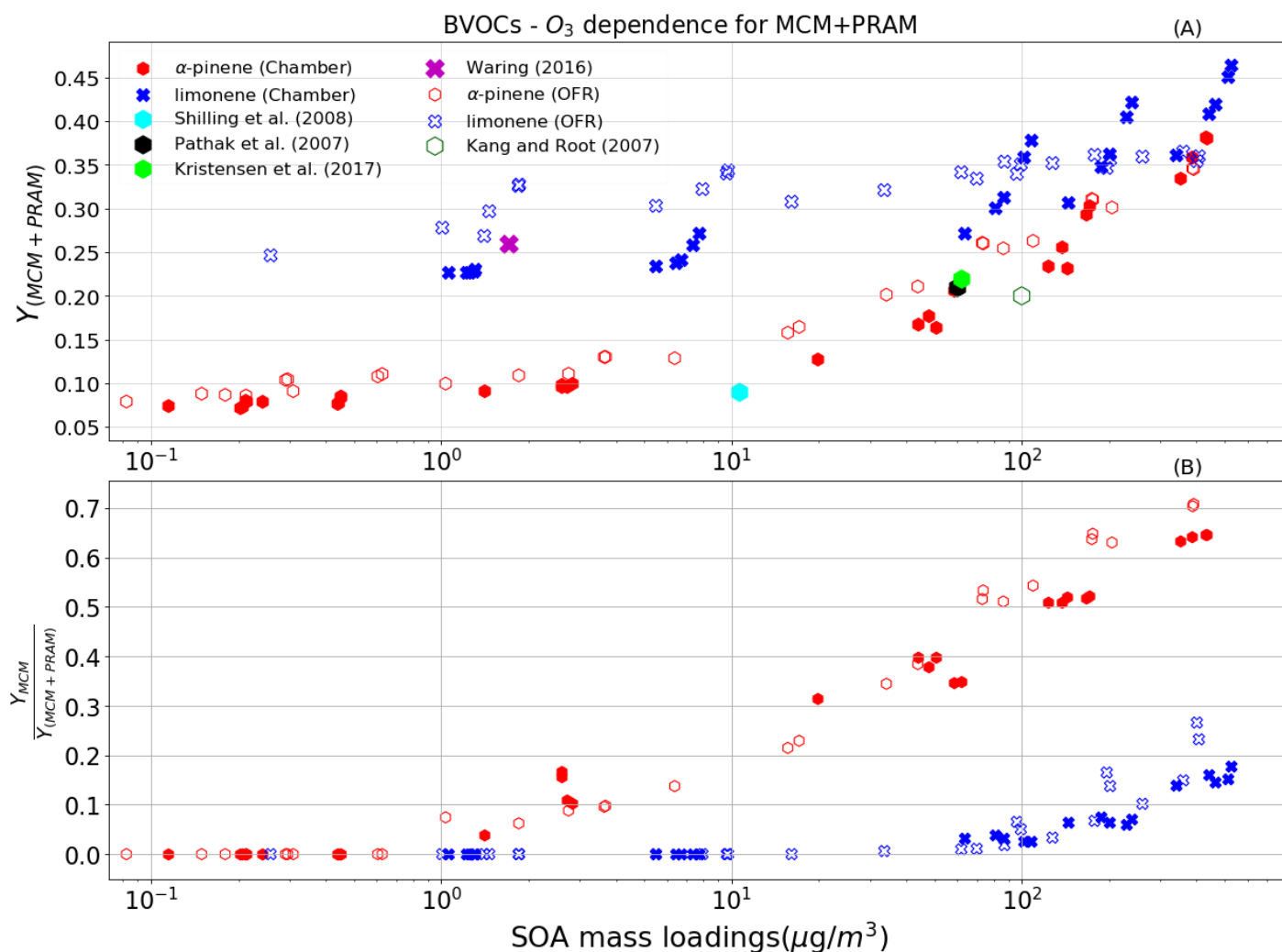
| SOA mass loading ($\mu\text{g m}^{-3}$) | MCM + PRAM mass yields range | MCM mass yields range | BVOC | Experimental yields | References |
|---|------------------------------|-----------------------|------------------------|-----------------------|--------------------------|
| 0– 15 [†] | 0.07– 0.08 | 0.00 – 0.06 | α -pinene | 0.09 (10.6) | Shilling et al. (2008) |
| 16 - 60 [†] | 0.12 – 0.20 | 0.06 – 0.11 | α -pinene | 0.16 – 0.21 (15 -60) | Pathak et al. (2007) |
| 61 – 200 [†] | 0.22 – 0.30 | 0.12 – 0.15 | α -pinene | 0.22 (62) | Kristensen et al. (2017) |
| 1.1– 550 [†] | 0.24 -0.48 | 0.007-0.06 | limonene | 0.26 (1.7) | Waring (2016) |
| 0 - 100 [†] | 0 – 0.09 ^{!!} | 0 – 0.09 | β -pinene | 0.03-0.22 (7.2 - 100) | Griffin (1999) |
| 0 -10 [†] | 0 – 0.01 ^{!!} | 0 – 0.01 | β -caryophyllene | 0.13 (1.8) | Chen et al. (2012) |

246 ^{!!}indicates that no PRAM mechanism available yet i.e the yields are same as the MCM yields.

Table 2b. Mass yields for BVOCs ozonolysis at 293 K for different range of mass loadings using an OFR^{||} setup.

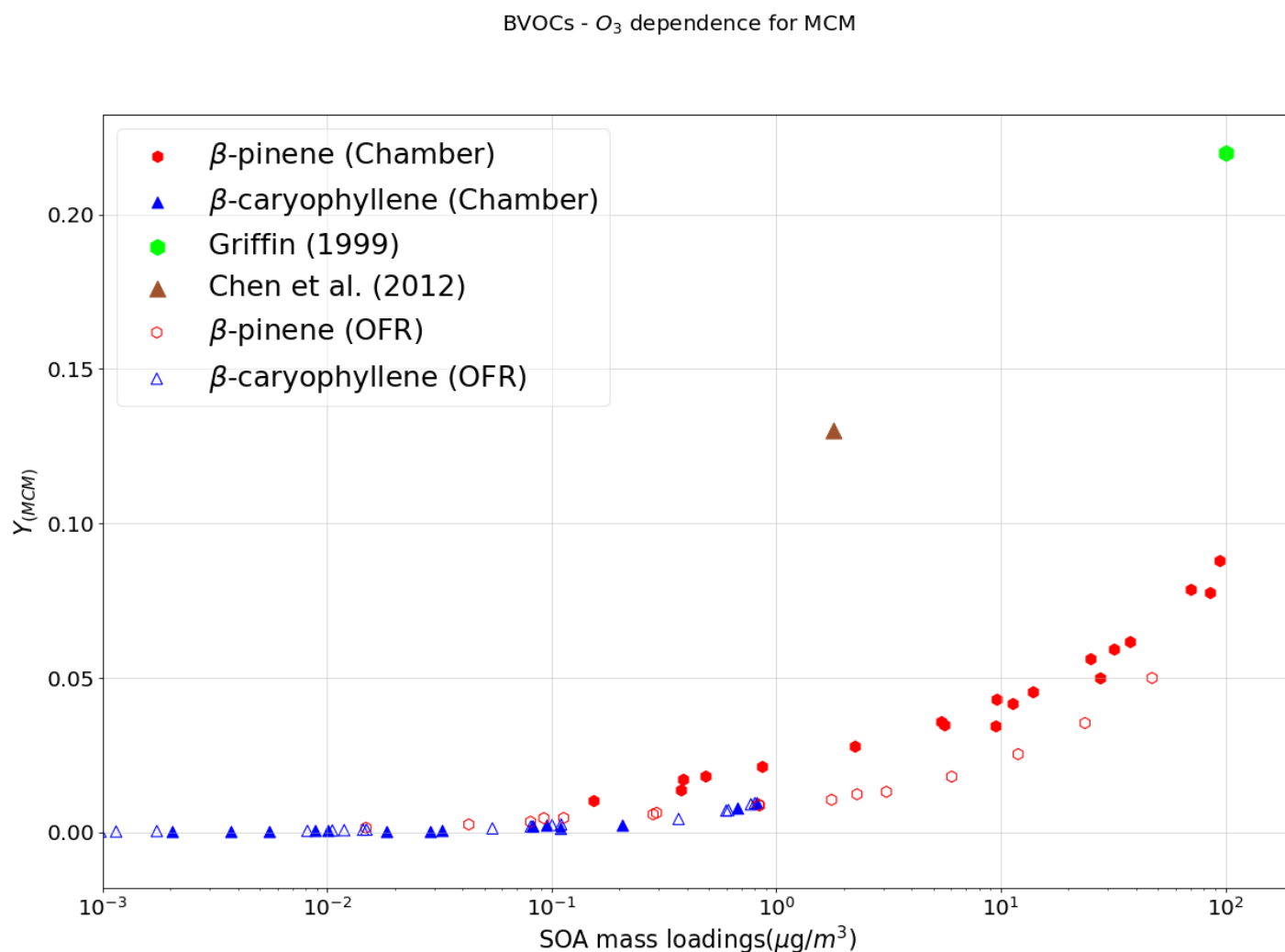
| SOA mass loading (ppb) | MCM + PRAM mass yields range | MCM mass yields range | BVOC | Experimental yields | References |
|------------------------|------------------------------|-----------------------|------------------|---------------------|----------------------|
| 0-100 | 0.07-0.25 | 0-0.13 | α -pinene | 0.2 (100) | Kang and Root (2007) |
| 0-156 | 0 – 0.02 | 0 – 0.02 | β -pinene | 0.49 (156) | Kang and Root (2007) |

247 ^{||}indicates that no PRAM mechanism available yet i.e the yields are same as the MCM yields.



248 **Figure 1.** The mass yields from the ozonolysis of BVOCs α -pinene (red heptagon) and limonene (blue crosses) modelled after
 249 chamber (filled symbols) and flow-tube settings (open symbols). The figure shows a comparison of SOA mass yields obtained from
 250 simulations with MCM + PRAM (panel A) and ratio of yields from MCM and MCM+PRAM (panel B). Currently PRAM is

251 available for **ozonolysis** of limonene and α -pinene. The clumps are a result of SOA mass yields for the oxidation of specific
 252 oxidant concentration with varying BVOC concentration



254 **Figure 2.** The mass yields from the ozonolysis of BVOCs β -pinene and β -caryophyllene modelled after chamber (filled symbols)
 255 and flow-tube (open symbols) settings. The figure shows a comparison of SOA mass yields obtained from simulations with only
 256 MCM as currently there is no PRAM available for these compounds. The experimental values are provided for comparison.

257 3.2 BVOCs – OH chamber and flow-tube simulations

258 The mass yields obtained by MCM+PRAM for α -pinene – OH oxidation are close to the measured
 259 values (Kristensen et al., 2017), while using only MCM under-predicts the mass yields (Figure 3 , panel A
 260 and B, and Table 3). The maximum SOA mass yield for OH oxidation of α -pinene is lower than the yield
 261 from ozonolysis which is suspected to arise due to the formation of more volatile oxidation products produced
 262 during OH oxidation (Bonn and Moortgat, 2002; Kristensen et al., 2014). The OH oxidation of β -pinene
 263 results in mass yields similar to the measurements obtained by Lee et al. (2006b) for similar mass loadings.

264 The β -pinene SOA yields are comparatively well represented by MCM+PRAM in comparison to the
265 standalone MCM. On the other hand, the limonene mass yields are under-predicted by MCM+PRAM for
266 similar mass loadings. Yields for limonene SOA mass loadings of $350 \mu\text{g m}^{-3}$ are around 0.31 which is lower
267 than the experimental values of 0.58, measured by Lee et al. (2006b).

268 For β -caryophyllene, the modeled values are in good agreement with experimental measured yields in
269 the range of mass loadings provided by Griffin (1999) and Tasoglou and Pandis (2015). Currently there are no
270 experiments providing HOM yields from OH oxidation of β -caryophyllene, and hence, those species are not
271 included in PRAM. The simulation results for yields from OH oxidation of β -caryophyllene, indicate that the
272 MCM scheme is able to reproduce the experimental values (Fig. 4). Only MCM was used for modeling the
273 mass yields for OH oxidation of isoprene due to current lack of PRAM mechanism for isoprene. The mass
274 yields derived from OH oxidation of isoprene vary from 0.01 - 0.31 covering a range of mass loadings from
275 $0.003 - 132 \mu\text{g m}^{-3}$. At low mass loadings $< 10 \mu\text{g m}^{-3}$ the maximum yield obtained is ~ 0.06 , which is a factor
276 of 3 greater than the experimental results obtained by (Lee et al., 2006b) where they measured yield of 0.02.
277 The mass yields are in good agreement with the experimental results from Liu et al. (2016), wherein they
278 measured a yield of 0.13 for $22 \mu\text{g m}^{-3}$ (Table 3).

279 The OFR simulations results for the OH oxidation of BVOCs with an equivalent exposure range from
280 $2.0 \times 10^{10} - 2.0 \times 10^{12} \text{ molecules cm}^{-3} \text{ s}$, is shown in Fig. 3. Our yields for α -pinene agree well with the yields
281 obtained by Bruns et al. (2015) where they measured yield of ~ 0.3 for mass loading of $\sim 300 \mu\text{g m}^{-3}$ at
282 equivalent OH exposures. Friedman and Farmer (2018) found mass yields of 0 - 0.086 for α -pinene
283 (ammonium sulfate seeded experiment), 0- 0.12 for β -pinene (no seed particles) and 0-0.04 for limonene (no
284 seed particles), by varying the OH exposures between $4.7 \times 10^{10} - 7.4 \times 10^{11} \text{ molecules cm}^{-3} \text{ s}$. Our simulated
285 yields for OH oxidation of α -pinene, β -pinene and limonene suggest higher mass yields for α -pinene and
286 limonene at equivalent mass loadings, while mass yields for β -pinene are in good agreement with the
287 experimental yields. Friedman and Farmer (2018) suggest that the reason for this underestimation in mass
288 yields could arise due to the exclusion of large particle sizes in the experiments and propose that these yields
289 could represent lower bounds.

290

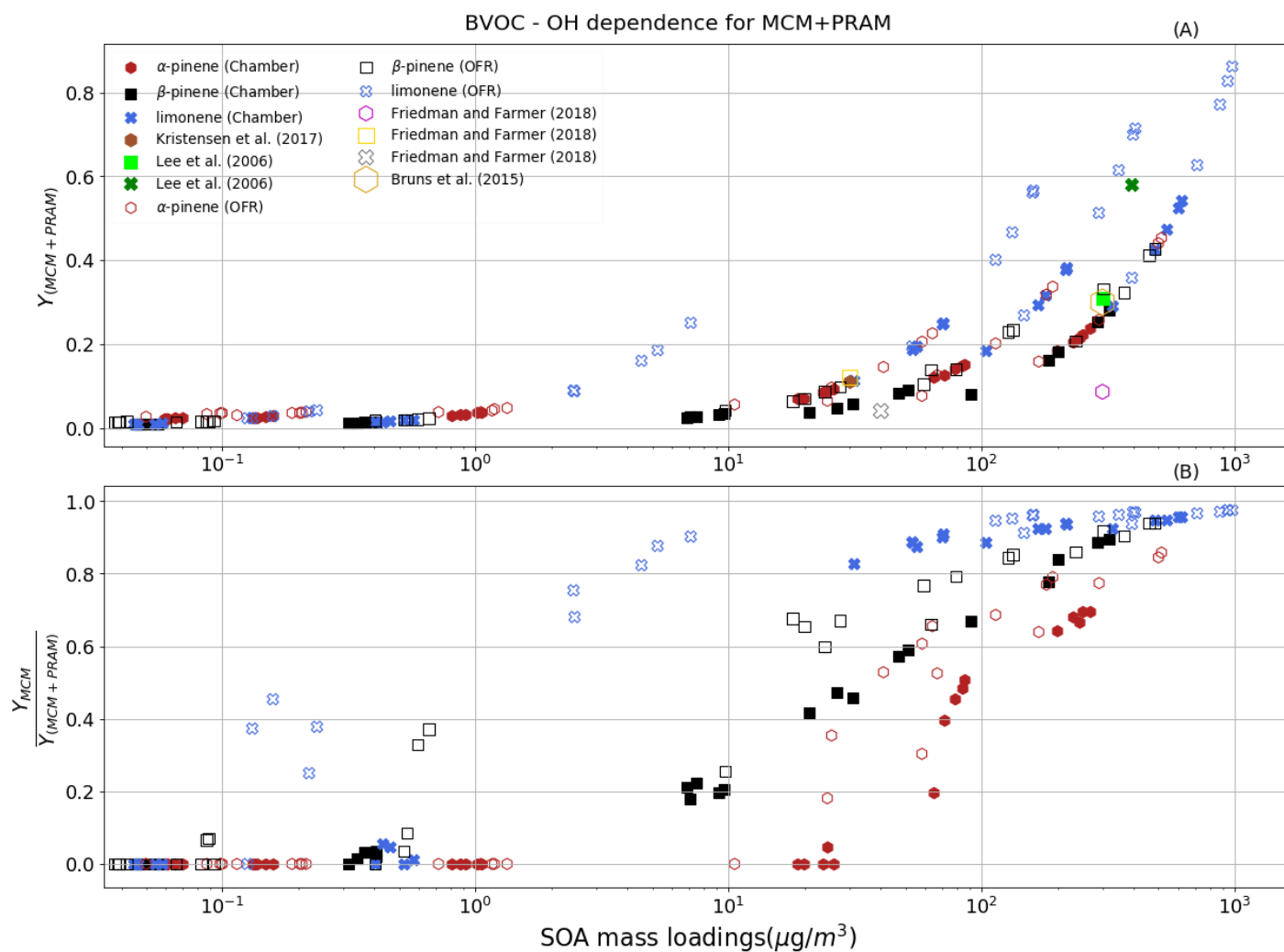
291

292

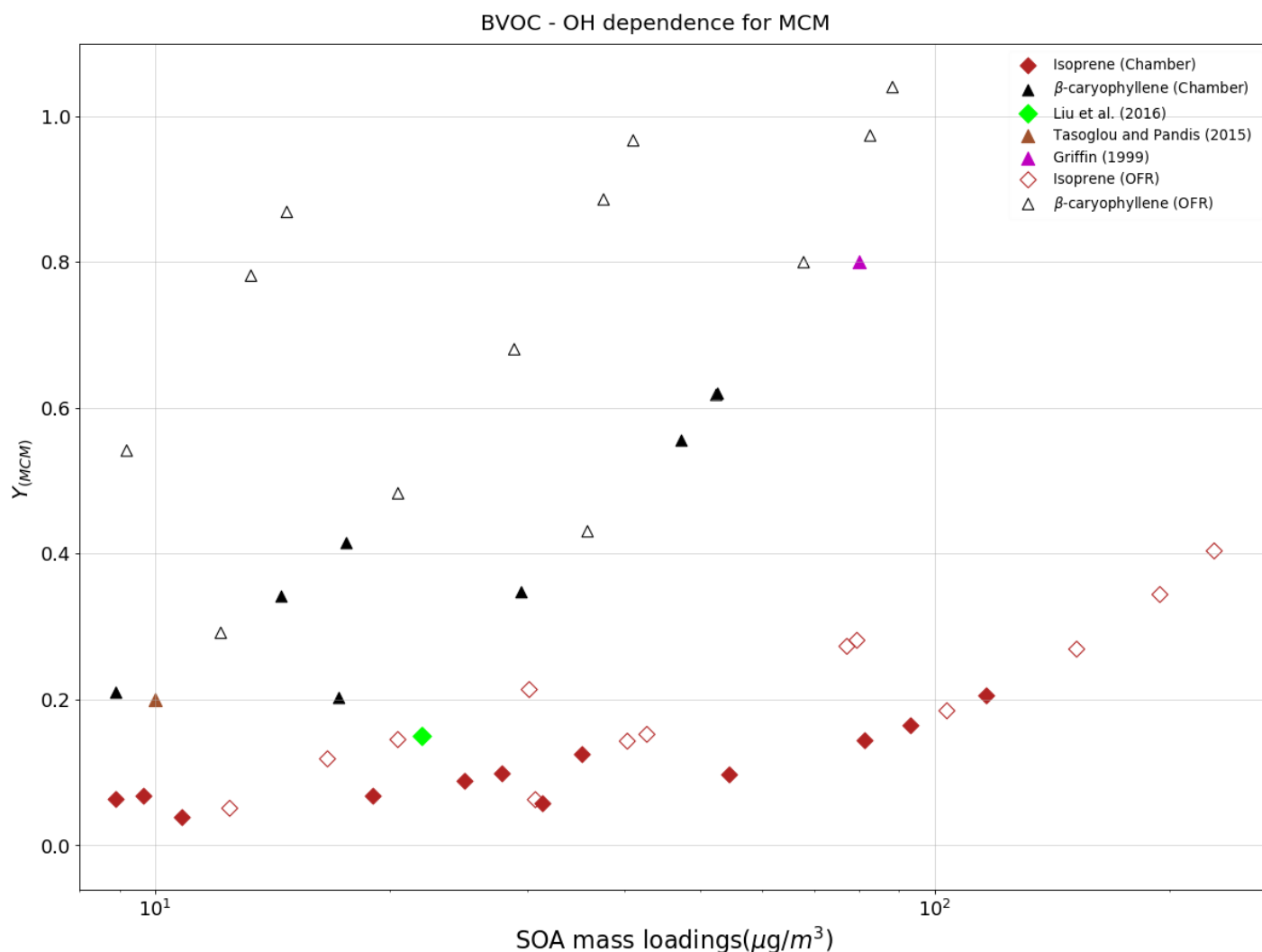
293 **Table 3.** Mass yields for OH oxidation of BVOCs at 293 K for different range of mass loadings using a
 294 chamber[†] and OFR[‡] setup.

| SOA mass loading ($\mu\text{g m}^{-3}$) | MCM + PRAM mass yields | MCM mass yields | BVOC | Experimental yields | References |
|---|------------------------|-----------------|------------------------|--------------------------------|---|
| 300 [†] | 0.28 | 0.25 | β -pinene | 0.31 (293) | Lee et al. (2006b) |
| 350 [†] | 0.31 | 0.06 – 0.11 | limonene | 0.58 (394) | Lee et al. (2006b) |
| 30 | 0.09 | 0.004 | α -pinene | 0.11 (30) | Kristensen et al., 2017 |
| < 10 [†] | 0.21 [‡] | 0.21 | β -caryophyllene | 0.2 (8.8) | Tasoglou and Pandis (2015) |
| 20 – 80 [†] | 0.3 – 0.7 [‡] | 0.3 – 0.7 | | 0.37 – 0.79 (17-82) | Griffin (1999) |
| 22 [†] | 0.1 [‡] | 0.1 | Isoprene | 0.13 (22) | Liu et al. (2016) |
| <10 | 0.06 [‡] | 0.06 | | 0.02 (9) | Lee et al. (2006b) |
| 0-300 [‡] | 0.05 – 0.31 | 0 – 0.2 | α -pinene | 0 – 0.086 (0-300) 0.3 (300) | Friedman and Farmer (2018) Bruns et al. (2015) |
| 0-30 [‡] | 0-0.1 | 0-0.01 | β -pinene | 0 – 0.12 (30) | Friedman and Farmer (2018) |
| 0-40 [‡] | 0.-0.19 | 0-0.17 | limonene | 0.0 – 0.04 (35) | Friedman and Farmer (2018) |

295 [‡]indicates that no PRAM mechanism available yet i.e the yields are same as the MCM yields.



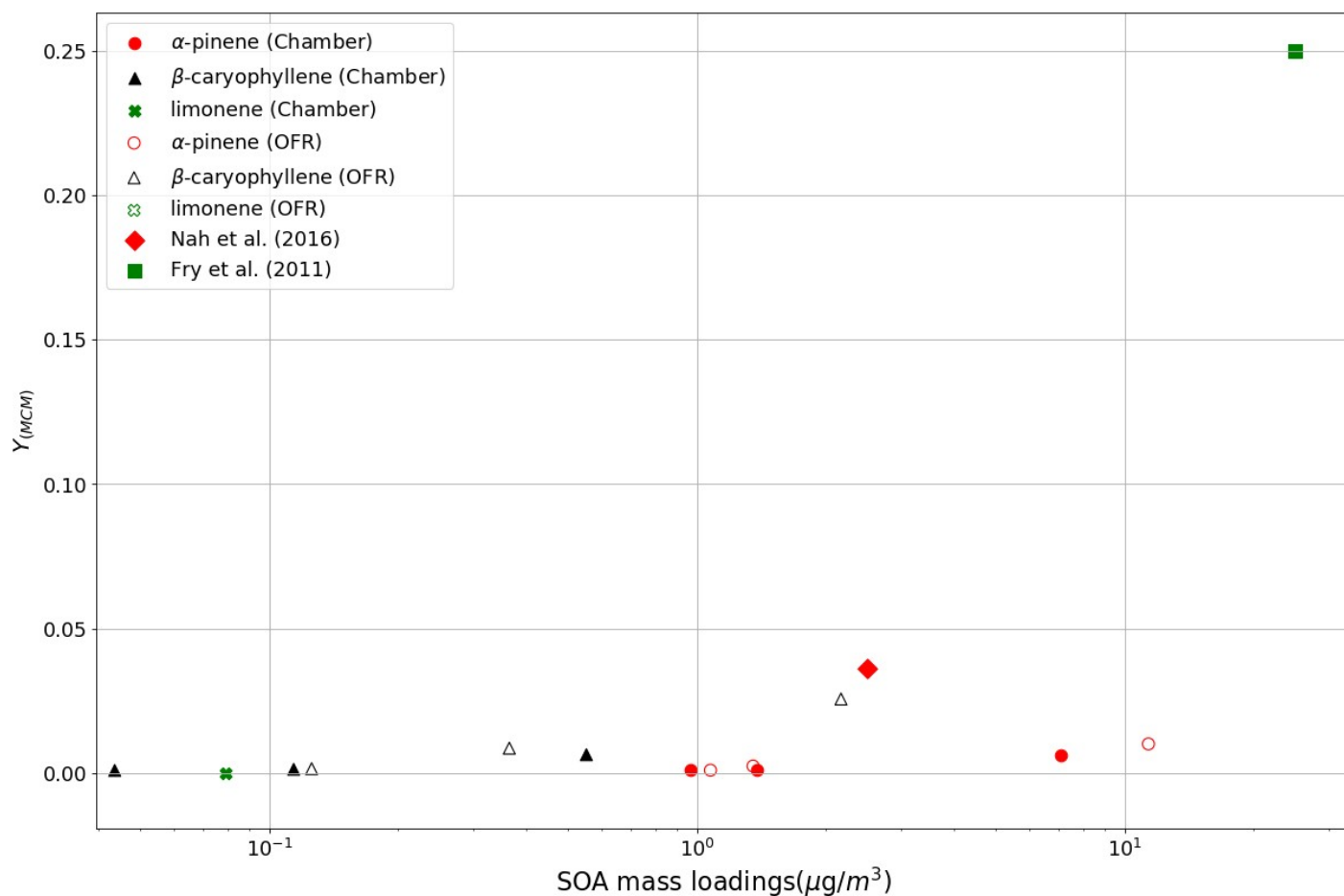
296 **Figure 3.** The mass yields from OH oxidation of BVOCs α -pinene (red heptagons), β -pinene (black squares) and limonene (blue
 297 crosses) modeled after chamber (filled symbols) and flow-tube settings (open symbols). The figure shows a comparison of SOA
 298 mass yields obtained from application of MCM+PRAM (panel A) and ratio of yields from MCM and couple MCM+PRAM (panel
 299 B). Currently PRAM is available for OH oxidation of limonene and α -pinene and β -pinene.



301 **Figure 4.** The mass yields from OH oxidation of BVOCs β -caryophyllene (black triangles) and isoprene (maroon diamonds)
 302 modeled after chamber (filled symbols) and flow-tube settings (open symbols). The figure shows a comparison of SOA mass yields
 303 obtained from application of MCM as currently there is no PRAM available for these compounds.

304 3.3 BVOC – NO₃ chamber and OFR simulations

305 Figure 5. shows the yields derived from the oxidation of BVOCs by NO₃. Currently, as no PRAM is
 306 available for NO₃ oxidation, Figure 5 represents SOA yields derived using MCM. Due to limited
 307 experimental constraints, PRAM presently does not consider autoxidation of RO₂ formed from NO₃ oxidation
 308 of VOCs, which could explain the huge discrepancy between the measured and simulated mass yields (Figure
 309 5). The yields obtained for oxidation of α -pinene (0.002-0.007) by NO₃ are low in comparison to those
 310 obtained by Nah et al. (2016), where they measured a yield of 0.036. Measured mass yields for limonene
 311 oxidation by NO₃ resulting in mass yields between 0.25-0.4 (Fry et al., 2011), whereas we obtain negligible
 312 (~ 0.0003) mass yields for the same.

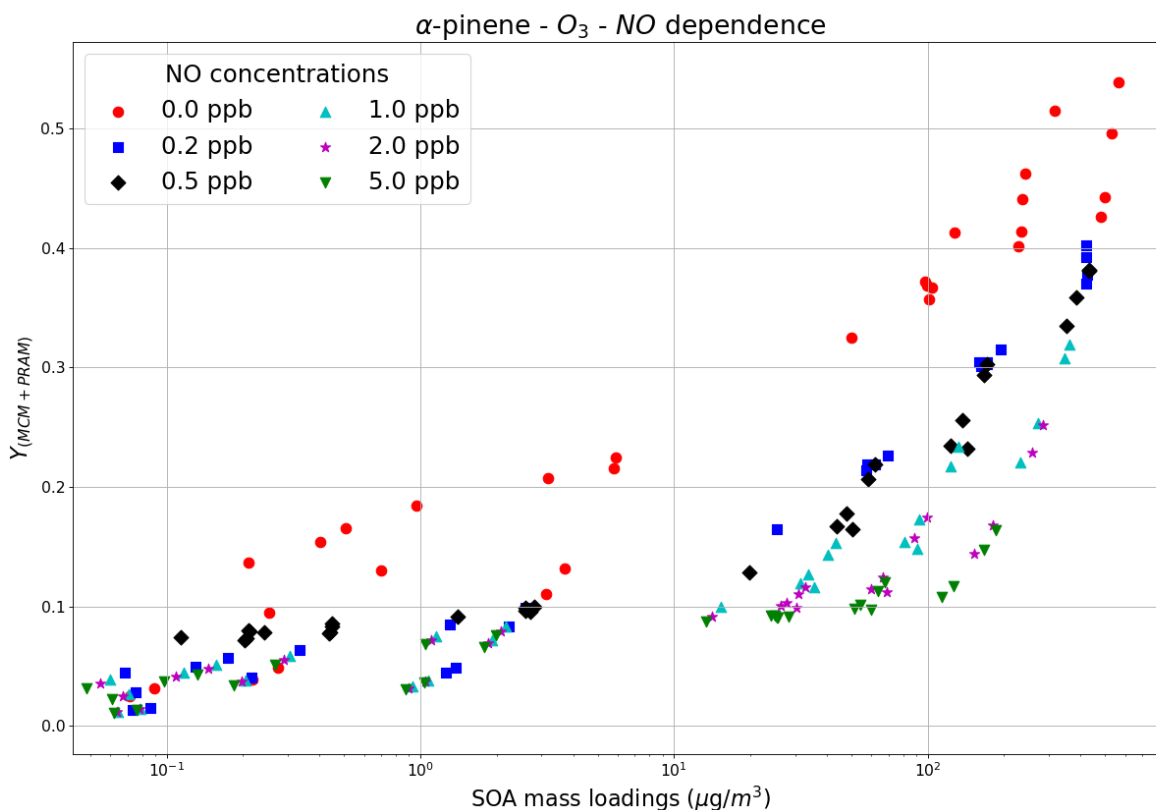
BVOC - NO_3 dependence for MCM

313 **Figure 5.** The mass yields from NO_3 oxidation of BVOCs modeled after chamber and flow-tube settings. The figure shows a
 314 comparison of SOA mass yields obtained from application of MCM. Appreciable mass yields were only obtained for α -pinene,
 315 limonene and β -caryophyllene.

316 3.4 NO_x dependence

317 Varying NO_x concentrations changes the fate of RO_2 radical formed during organic oxidations by
 318 altering HO_2/RO_2 ratio, thereby impacting the distribution of reaction products and aerosol formation (Presto
 319 et al., 2005; Zhao et al., 2018; Sarrafzadeh et al., 2016). We modeled the SOA mass yields for α -pinene - O_3
 320 setup with varying NO_x concentrations (NO was varied whereas NO_2 was kept constant for all the runs), for
 321 initial α -pinene mixing ratios in the range 0.5 - 200 ppb (Fig. 6). A maximum SOA yield value of 0.55 is
 322 obtained for a combination of the lowest value of NO (0 ppb, red circles). As the NO concentrations increase
 323 from 0.2 ppb (blue squares) to 5 ppb (green inverted triangles) the yields begin to decrease, and this pattern is
 324 observable and valid for all concentration ranges of reacted precursor VOC. The NO_x dependence of α -pinene

325 ozonolysis is consistent with the findings of Draper et al. (2015) and Presto et al. (2005) wherein they
 326 observed a trend of decreasing SOA mass yields for α -pinene ozonolysis with increasing NO_x concentrations.

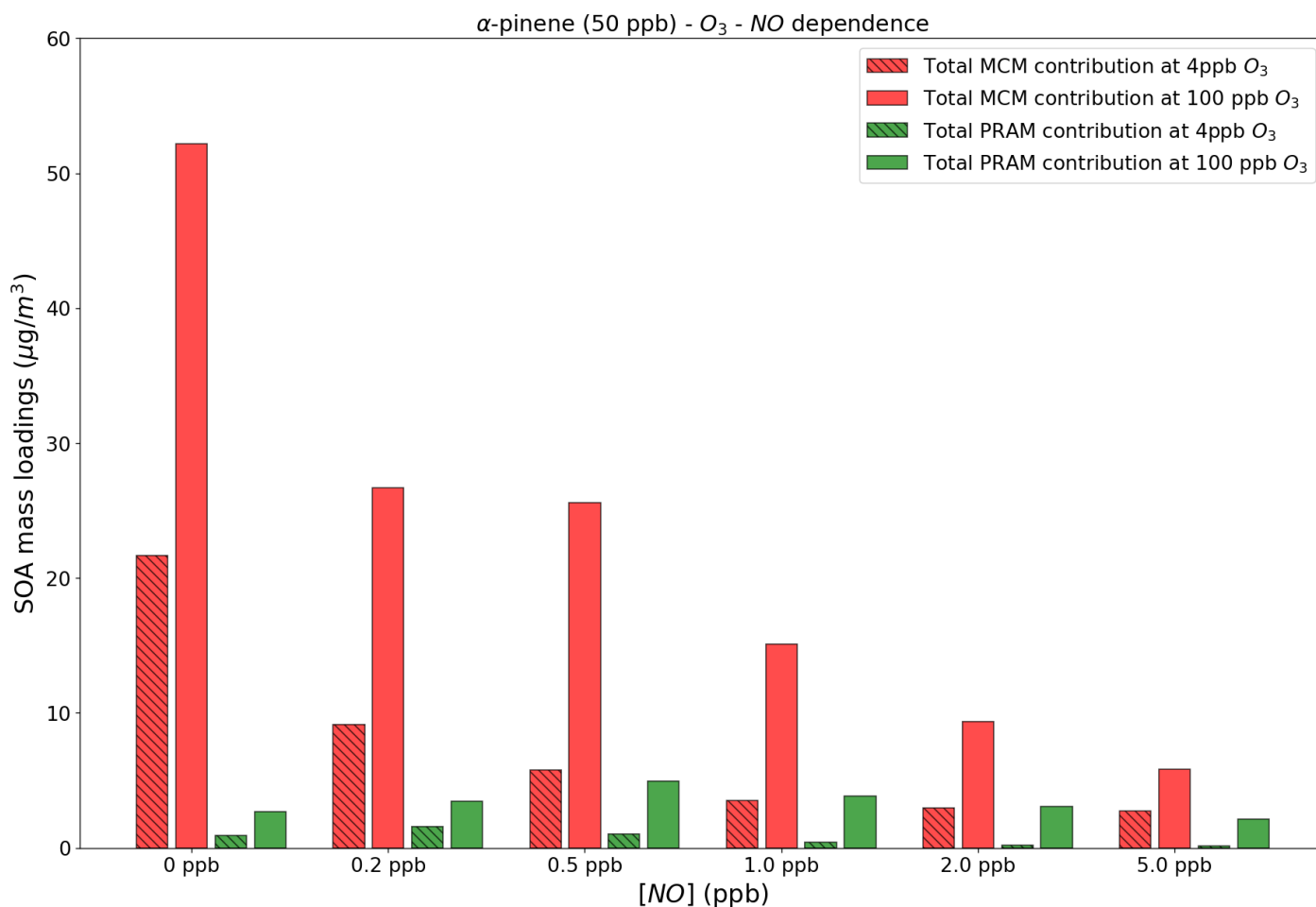


327 **Figure 6.** The SOA mass yields from O_3 oxidation of α -pinene modeled for different NO concentrations with the chamber setup.
 328 The model runs were performed using MCM+PRAM.

329 At low NO_x concentrations RO_2 radicals undergo rapid autoxidation until they react with HO_2 or RO_2
 330 resulting in production of low volatility hydro-peroxide products (Sarrafzadeh et al., 2016), closed shell
 331 monomers or dimers (Ehn et al., 2014; Roldin et al., 2019), which increase SOA mass. This contrasts with
 332 high NO_x conditions where the $\text{RO}_2 + \text{NO}$ reactions dominate over reactions with HO_2 or RO_2 , resulting in the
 333 formation of more volatile products such as aldehydes, ketones and organonitrates (Presto et al., 2005;
 334 Sarrafzadeh et al., 2016), and likely suppressing the autoxidation process leading to a decrease in SOA mass
 335 loadings (Ehn et al., 2014).

336 Figure 7 shows the absolute contributions to SOA mass loadings by PRAM and MCM compounds at
 337 two different O_3 concentrations of 4 and 100 ppb and varying NO concentrations. The figure shows that with
 338 an increase in NO concentrations more than 1 ppb the contribution of PRAM compounds to the particle phase

339 decreases at both 4 and 100 ppb of O₃ concentrations. In PRAM the RO₂ + NO reaction leads either to the
 340 formation of organonitrate HOM, closed shell monomers with carbonyl group or fragmentation products with
 341 higher volatility (Roldin et al., 2019). HOM Dimer formation is suppressed with increasing NO
 342 concentrations in PRAM (Roldin et al., 2019) which explains the lower contribution by PRAM compounds to
 343 SOA mass loadings with increasing NO. At NO concentrations <1ppb the PRAM contribution increases as,
 344 first generation RO₂ are capable of undergoing autoxidation forming highly oxygenated RO₂ which
 345 subsequently reacts with NO forming organic nitrates (Ehn et al., 2014). As NO concentrations exceed 1ppb
 346 the first generation RO₂ is scavenged by NO thereby reducing the concentration of organonitrate HOM (Ehn
 347 et al., 2014), possibly affecting SOA yields. The MCM contribution also decreases with increasing NO
 348 concentrations mostly due to the formation of more volatile organonitrates (Jenkin et al., 2019) .



349 **Figure 7.** Contribution to the SOA mass loadings by total PRAM and MCM compounds at different NO levels and O₃
 350 concentrations. For comparison we use 4 ppb and 100 ppb O₃ concentrations, respectively, at 50 ppb α-pinene.

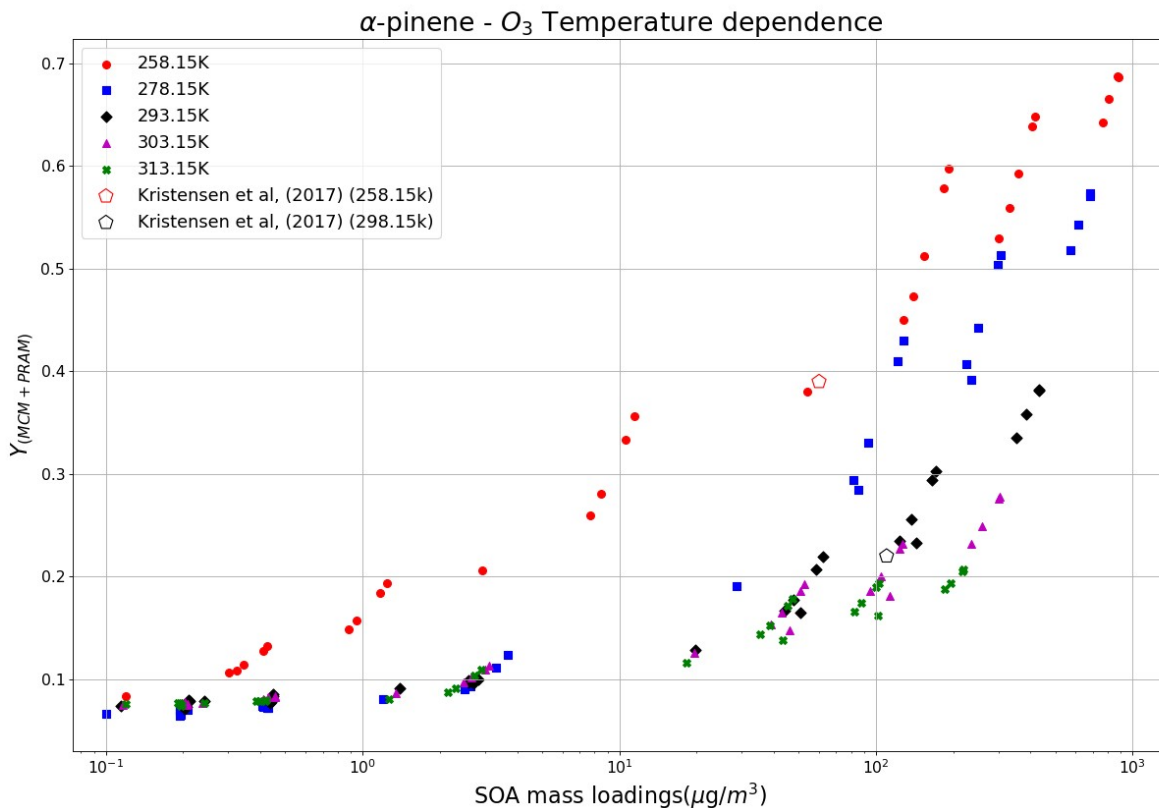
351

352

353 3.5 Temperature dependence

354 The formation of SOA from α -pinene ozonolysis in the temperature range of 258.15 - 313.15 K was
355 investigated in this study using MCM+PRAM. Strong dependence of SOA mass yield on temperature was
356 reported by Saathoff and Naumann, (2009) wherein they measured the decreasing mass yields from 0.42 at
357 273.15 K to 0.09 to 313.15 K for SOA loadings of 53 and 92 $\mu\text{g m}^{-3}$ respectively. Our results in Figure 8
358 show increasing SOA mass yields for α -pinene ozonolysis with decreasing temperature, which is attributed to
359 the augmented condensation of oxidation products termed as semi volatile organic compounds (SVOC)
360 (Kristensen et al., 2017) at lower temperatures.

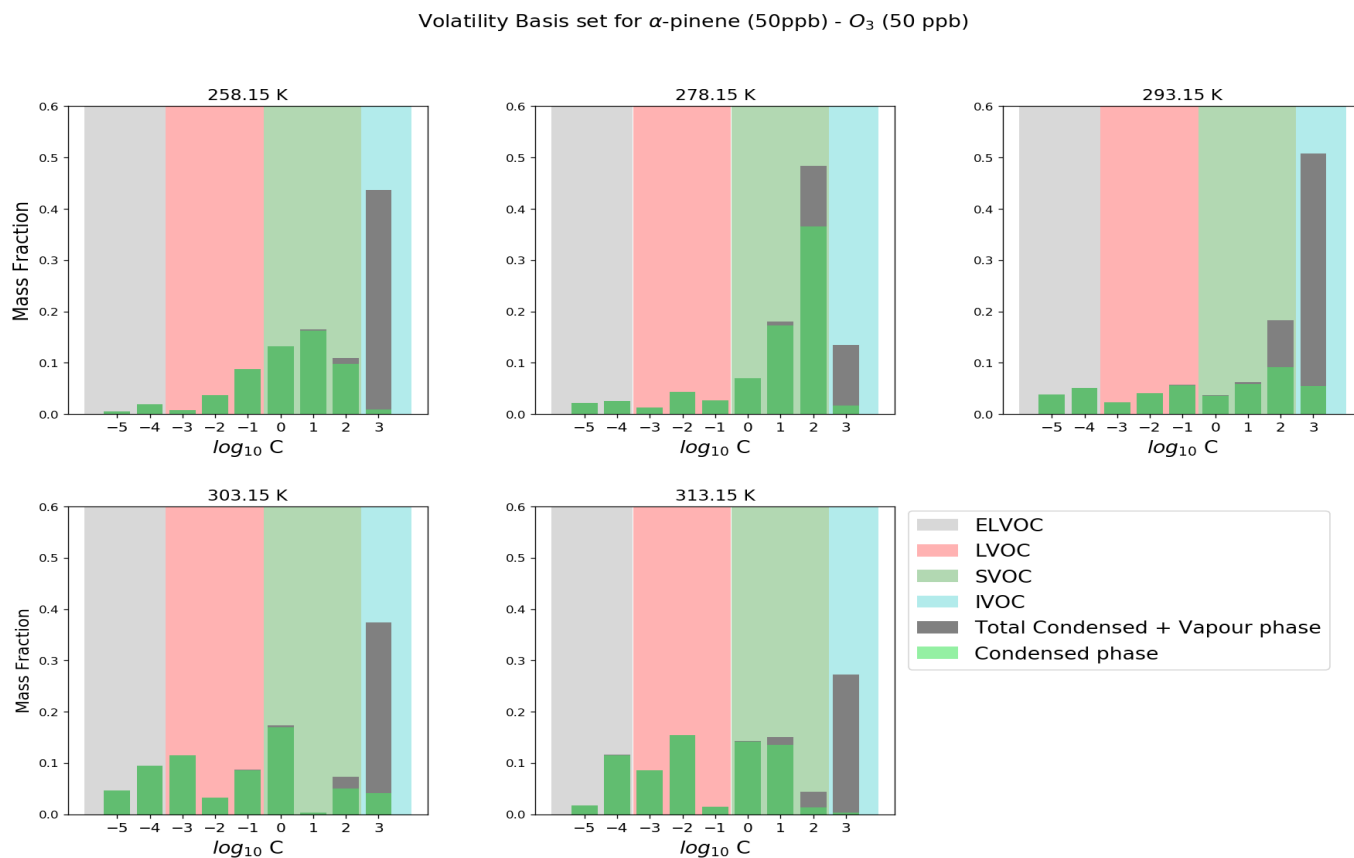
361 For α -pinene maximum mass loading $< 150 \mu\text{g m}^{-3}$ the mass yields reach a maximum value of 0.38 at
362 temperatures as low as 258.15 K and decrease to 0.27 for a temperature of 293.15 K and to 0.1 for the
363 temperature of 313.15 K. These yields are comparable to the results obtained by Kristensen et al.
364 (2017) where they measured yields of 0.39 for 258.15 K and 0.22 for 293.15 K for mass loading $< 150 \mu\text{g m}^{-3}$.
365 The results show a weak dependence of SOA mass yields on temperatures in the range of 278.15 K - 313.15
366 K at low SOA mass loadings which become more pronounced as the mass loadings increase. At the lowest
367 temperature of 258.15 K the mass yields are higher in comparison to other temperatures regardless the mass
368 loadings. These results are in good agreement with the findings by Pathak et al. (2007) where they found a
369 strong temperature dependence of SOA mass yields at lower temperature (0 – 15° C), which decreases as the
370 temperature increases. Furthermore, similar to the measurements made by Pathak et al. (2007), our
371 simulations were able to reproduce the experimental findings that show no appreciable differences in the SOA
372 mass yields for loadings below 1 $\mu\text{g m}^{-3}$ (initial mixing ratio of 1 ppb) for temperatures > 273.15 K.



373 **Figure 8.** Temperature dependence of SOA mass yields at different temperatures using the MCM+PRAM. The open pentagons
 374 represent measurement data from Kristensen et al. (2017) at 258.15 K and 298.15 K.

375 Figure 9 shows the volatility distribution of α -pinene ozonolysis derived SOA at different
 376 temperatures. The saturation vapor pressure limits for defining extremely low volatility (ELVOCs - grey
 377 shaded), low volatility (LVOCs - red shaded), semi volatile (SVOCs - green shaded) and intermediate
 378 volatility (IVOCs - cyan shaded) organic compounds used in the Volatility basis set (VBS) are set according
 379 to the values suggested in Donahue et al. (2012). In this work, we categorize compounds (ELVOCs, LVOCs,
 380 SVOCs and IVOCs) based on effective saturation vapor pressures (C^*) in the range of $\{10^{-5}$ to $10^3\}$ $\mu\text{g m}^{-3}$
 381 and temperature of 298 K (Donahue et al., 2009). At the lowest temperature of 258.15 K, the SVOCs
 382 contribution to the particle phase is dominant in comparison to LVOCs and ELVOCs, a trend which is
 383 subsequently reversed as the temperatures are increased. At 293.15 K a majority of SVOCs and IVOCs are in
 384 the gas phase while the contribution of LVOCs and ELVOCs to particle phases increases. These results are in
 385 good agreement with observations made by Kristensen et al. (2017) wherein they observed an increasing
 386 contribution of SVOCs at sub-zero temperatures of 258.15 K, which decrease the fraction of SOA formed

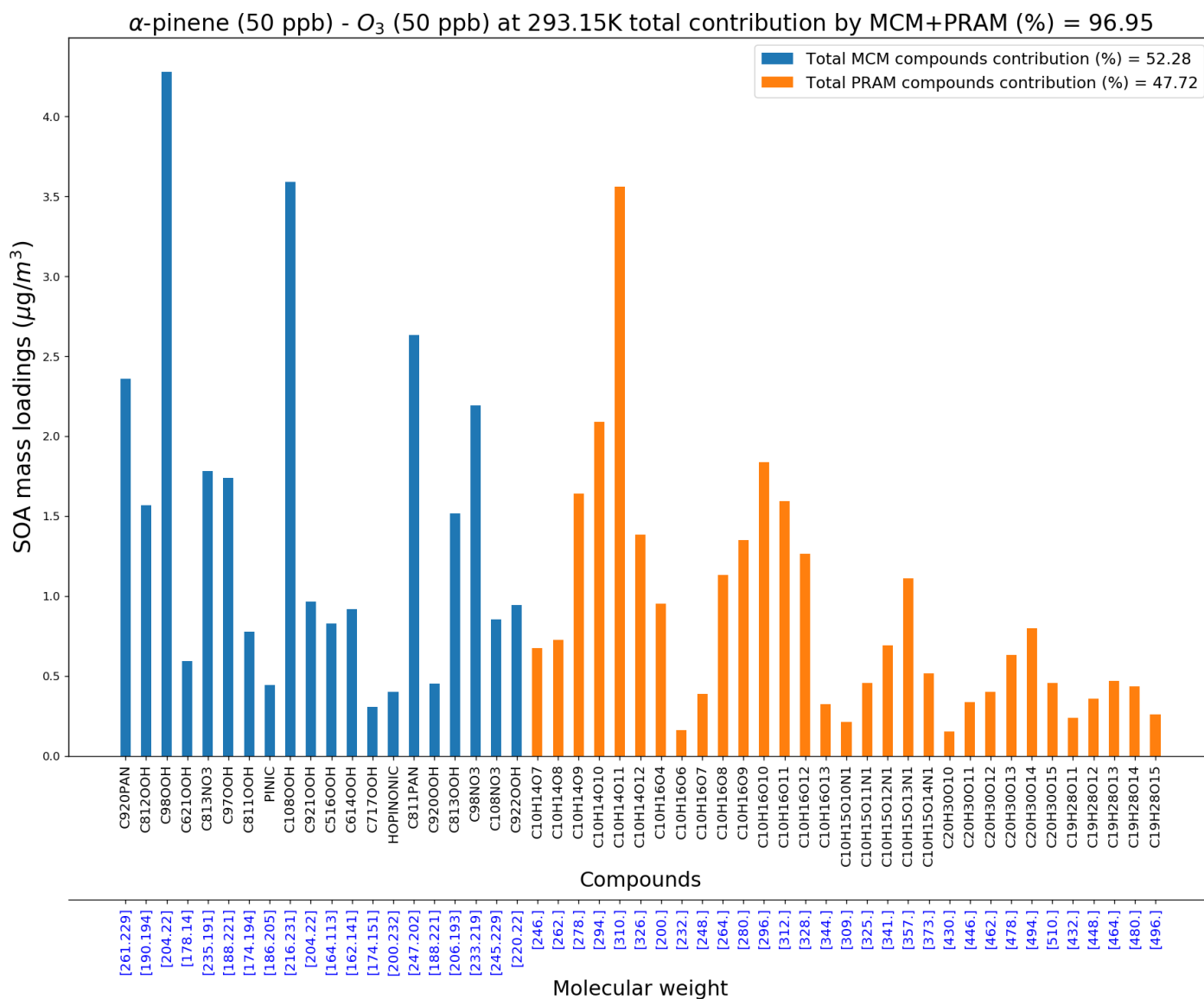
387 from ELVOCs. Again, it should be noted that the temperature dependence of peroxy radical autoxidation
 388 product formation still needs further validation based on recent experiments (e.g. Quéléver et al., 2019).
 389



390 **Figure 9.** Modeled volatility distribution of SOA at different temperatures. The volatility bins span a range of effective saturation
 391 vapor pressures $C = C^* = \{10^{-5} \text{ to } 10^3\} \mu\text{g m}^{-3}$. The VBS distribution is based on a reference temperature of 298 K.

392 3.6 Composition

393 MCM+PRAM can be used to narrow down and compile a list of compounds playing a pivotal role in
 394 contributing to SOA mass loadings and, also compare the relative importance of implementing PRAM
 395 alongside the MCM. Figure 10 shows the most important compounds from both the MCM and PRAM that
 396 together contribute to more than 95% of α -pinene ozonolysis SOA mass loading at 293.15 K.



397 **Figure 10.** MCM and PRAM Compounds contributing to > 95 % of SOA mass at 293 K and 50ppb O_3 and α -pinene
 398 concentrations.

399 Figure 10 shows that contribution to SOA mass loadings by PRAM compounds is ~48 % (of 97 %) while
 400 MCM compounds contribute ~52 % (of 97%). On lowering the temperature to 258K the relative contributions
 401 of PRAM drop to 15 % (of ~99 %), while MCM dominates by contributing ~85 % (of ~99 %) respectively
 402 (Figure S3a). The contribution of PRAM increases to ~64 % (of ~97 %) and MCM contribution drops to 36
 403 % (of ~97 %) at 313 K (Figure S3b). These results reflect the importance of PRAM as its contribution plays
 404 an increasingly dominant role with increasing temperatures and highlights the crucial few compounds that
 405 contribute to maximum SOA mass loadings for α -pinene ozonolysis. The list of abundant compounds which
 406 together add up to contribute more than 95 % of SOA mass loadings at 258 K, 293 K and 313 K are presented
 407 in the supplement Table 1s (a, b & c). At 258 K MCM compounds namely pinonic acid ($C_{10}H_{16}O_3$, 4.4 %),

408 C920PAN ($C_{10}H_{15}NO_7$, 9.3 %), C108NO3 ($C_{10}H_{15}NO_6$, 8.9 %), C811PAN ($C_9H_{13}NO_7$, 10.1 %), C717NO3
409 ($C_7H_9NO_6$, 11.3 %) contribute significantly to the total SOA mass loadings while PRAM compounds such as
410 $C_{10}H_{14}O_7$ (0.88 %), $C_{10}H_{16}O_4$ (1.3 %), $C_{10}H_{16}O_6$ (1.13 %) contribute significantly less. An increase in
411 temperature to 293 K results in an overall increase in contribution by PRAM compounds, with $C_{10}H_{14}O_{10}$ (3.6
412 %), $C_{10}H_{14}O_{11}$ (6.2 %), $C_{10}H_{16}O_{10}$ (3.2 %) playing an important role in contributing to the SOA mass loadings.
413 This trend of relative increase in the contribution by PRAM compounds over MCM compounds to SOA mass
414 loadings is also evident as the temperatures are further increased to 313 K, where the PRAM compounds
415 $C_{10}H_{14}O_{11}$ (18.3 %), $C_{10}H_{14}O_{12}$ (6 %) and $C_{10}H_{16}O_{12}$ (6.6 %) play a dominant role in increasing SOA mass
416 loadings.

417 4. Conclusions

418 We simulated SOA mass yields derived from the oxidation of various BVOCs (isoprene, α -pinene, β -
419 pinene, limonene and β -caryophyllene), by the oxidants O_3 , OH and NO_3 using the zero-dimensional model
420 MALTE-Box. The gas phase chemistry was simulated using the MCM in conjunction with PRAM. The aim
421 was to verify the efficacy of MCM+PRAM in simulating the SOA mass yields. Additional simulations were
422 performed to test the MCM+PRAM under varying temperature and NO concentrations. A few important
423 compounds playing a major role in increasing the SOA mass yields for α -pinene ozonolysis at different
424 temperatures are also highlighted.

425 The simulations were designed to resemble ideal smog chambers experiments and experiments in
426 oxidative flow reactors (OFR). No interactions between the gas phase and chamber walls were considered
427 during the simulations. For the smog chamber setting, the standalone MCM generally under-predicts the mass
428 yields obtained by the ozonolysis and OH oxidation of BVOCs. In contrast, the yields derived using
429 MCM+PRAM for the smog chamber setup is in good agreement with the experimental results. For an
430 idealized OFR setup, MCM+PRAM yields are in good agreement with experimental yields, while again the
431 MCM under-predicts the SOA yields. The relative contribution of HOM monomers and dimers to the particle
432 phase in OFR simulations is low when compared to the chamber simulations. This is due to higher RO_2
433 concentrations in OFR leading to termination of peroxy radical autoxidation, thereby affecting SOA yields.
434 This needs to be considered when applying yields based on OFR simulations in regional or global chemical
435 transport models

436 The model does not simulate appreciable SOA mass yields for oxidation of BVOCs with NO_3 , as
437 PRAM currently does not consider autoxidation of RO_2 formed from NO_3 oxidation of VOCs. This underlines
438 the need for developing a NO_3 oxidation scheme which can better constrain and predict SOA mass yields. In

439 accordance to the previous studies, the simulated SOA yields tend to decrease at higher temperatures. The
440 PRAM contribution to mass yields at low temperatures (258.15 K) is ~14 %, which is substantially lower than
441 that of MCM (~86 %). As the temperature is increased to 313.15 K, the contribution of PRAM to SOA mass
442 yields begins to dominate over MCM. This most likely is due to MCM producing more SVOCs (compounds
443 classified as SVOCs at 298 K), which show stronger contribution to particle phase at lower temperatures, due
444 to decrease in saturation vapor pressures with temperature. It should be noted that the present temperature
445 dependency of mass yields using PRAM are a first, and currently the best estimate in understanding the
446 influence of temperature on the peroxy radical autoxidation formation. The simulated SOA yields with
447 varying NO concentrations agree well with experimental results, i.e. SOA yields decrease with increasing NO
448 concentrations due to the formation of more volatile compounds such as organonitrates and ketones.

449 Using PRAM coupled with MCM helps us bridge the gap in understanding the role and contribution
450 of peroxy radical autoxidation to SOA formation. The variation of SOA yields for temperature and NO
451 concentrations, indicates the limitations of global and regional models in predicting e.g. cloud condensation
452 nuclei (CCN) effects using fixed SOA yields. The good agreement of modeled and experimental yields from
453 smog chambers, could further help us parameterize the SOA yields, that could be applied at a global and
454 regional model scale, to more accurately predict the direct and indirect impact of aerosol particles on e.g.
455 radiation balance by aerosol scattering/absorption and CCN concentrations. Furthermore, implementation of a
456 condensed PRAM version to regional and global models has been tested but still need further validation
457 (Roldin et al., 2019).

458 **Data availability**

459 The complete PRAM mechanism written in a format compatible with the Kinetic PreProcessor (KPP) together
460 with all species information can also be downloaded from <https://doi.org/10.1594/PANGAEA.905102>
461

462 **Author Contributions**

463 CX and MB served as the chief authors and editors of the paper. CX was performing the model simulations.
464 The study was designed by CX, MB and PR. All other co-authors contributed to the analysis and writing of
465 the paper.

466 **Acknowledgements**

467 The presented research has been funded by the Academy of Finland (Center of Excellence in Atmospheric
468 Sciences) grant no. 4100104 and the Swedish Research Council FORMAS, project no. 2018-01745. We
469 would also like to acknowledge the invaluable contribution of computational resources from CSC – IT Center
470 for Science, Finland.

471 **References**

- 472 Ahlberg, E., Eriksson, A., Brune, W. H., Roldin, P. and Svenningsson, B.: Effect of salt seed particle surface
473 area, composition and phase on secondary organic aerosol mass yields in oxidation flow reactors, *Atmos.*
474 *Chem. Phys.*, 19(4), 2701–2712, doi:10.5194/acp-19-2701-2019, 2019.
- 475 Berndt, T., Richters, S., Jokinen, T., Hyttinen, N., Kurtén, T., Otkjær, R. V., Kjaergaard, H. G., Stratmann, F.,
476 Herrmann, H., Sipilä, M., Kulmala, M. and Ehn, M.: Hydroxyl radical-induced formation of highly oxidized
477 organic compounds, *Nat. Commun.*, 7(May), doi:10.1038/ncomms13677, 2016.
- 478 Bianchi, F., Garmash, O., He, X., Yan, C., Iyer, S., Rosendahl, I., Xu, Z., Rissanen, M. P., Riva, M., Taipale,
479 R., Sarnela, N., Petäjä, T., Worsnop, D. R., Kulmala, M., Ehn, M. and Junninen, H.: The role of highly
480 oxygenated molecules (HOMs) in determining the composition of ambient ions in the boreal forest, *Atmos.*
481 *Chem. Phys.*, 17(22), 13819–13831, doi:10.5194/acp-17-13819-2017, 2017.
- 482 Bianchi, F., Kurtén, T., Riva, M., Mohr, C., Rissanen, M. P., Roldin, P., Berndt, T., Crouse, J. D.,
483 Wennberg, P. O., Mentel, T. F., Wildt, J., Junninen, H., Jokinen, T., Kulmala, M., Worsnop, D. R., Thornton,
484 J. A., Donahue, N., Kjaergaard, H. G. and Ehn, M.: Highly Oxygenated Organic Molecules (HOM) from Gas-
485 Phase Autoxidation Involving Peroxy Radicals: A Key Contributor to Atmospheric Aerosol, *Chem. Rev.*,
486 doi:10.1021/acs.chemrev.8b00395, 2019.
- 487 Bonn, B. and Moortgat, G. K.: New particle formation during α - and β -pinene oxidation by O₃, OH and NO₃,
488 and the influence of water vapour: Particle size distribution studies, *Atmos. Chem. Phys.*, 2(3), 183–196,
489 doi:10.5194/acp-2-183-2002, 2002.
- 490 Boy, M., Hellmuth, O., Korhonen, H., Nilsson, E. D., Revelle, D., Turnipseed, A., Arnold, F. and Kulmala,
491 M.: MALTE - Model to predict new aerosol formation in the lower troposphere, *Atmos. Chem. Phys.*, 6(12),
492 4499–4517, doi:10.5194/acp-6-4499-2006, 2006.
- 493 Bruns, E. A., El Haddad, I., Keller, A., Klein, F., Kumar, N. K., Pieber, S. M., Corbin, J. C., Slowik, J. G.,
494 Brune, W. H., Baltensperger, U. and Prévôt, A. S. H.: Inter-comparison of laboratory smog chamber and flow
495 reactor systems on organic aerosol yield and composition, *Atmos. Meas. Tech.*, 8(6), 2315–2332,
496 doi:10.5194/amt-8-2315-2015, 2015.
- 497
- 498 Chen, Q., Li, Y. L., McKinney, K. A., Kuwata, M. and Martin, S. T.: Particle mass yield from β -
499 caryophyllene ozonolysis, *Atmos. Chem. Phys.*, 12(7), 3165–3179, doi:10.5194/acp-12-3165-2012, 2012.
- 500 Crouse, J. D. and Nielsen, L. B.: Autoxidation of Organic Compounds in the Atmosphere, *J. Phys. Chem.*
501 *Lett.*, 24(4), 3513–3520, doi:10.1021/jz4019207, 2013.
- 502 Damian, V., Sandu, A., Damian, M., Potra, F. and Carmichael, G. R.: The kinetic preprocessor KPP - A
503 software environment for solving chemical kinetics, *Comput. Chem. Eng.*, 26(11), 1567–1579,
504 doi:10.1016/S0098-1354(02)00128-X, 2002.
- 505 Donahue, N. M., Robinson, A. L., Stanier, C. O. and Pandis, S. N.: Coupled Partitioning, Dilution, and
506 Chemical Aging of Semivolatile Organics, *Environ. Sci. Technol.*, 40(8), 2635–2643, doi:10.1021/es052297c,
507 2006.
- 508 Donahue, N. M., Robinson, A. L. and Pandis, S. N.: Atmospheric organic particulate matter: From smoke to
509 secondary organic aerosol, *Atmos. Environ.*, 43(1), 94–106,
510 doi:https://doi.org/10.1016/j.atmosenv.2008.09.055, 2009.

- 511 Donahue, N. M., Kroll, J. H., Pandis, S. N. and Robinson, A. L.: A two-dimensional volatility basis set-Part 2:
512 Diagnostics of organic-aerosol evolution, *Atmos. Chem. Phys.*, 12(2), 615–634, doi:10.5194/acp-12-615-
513 2012, 2012.
- 514 Draper, D. C., Farmer, D. K., Desyaterik, Y. and Fry, J. L.: A qualitative comparison of secondary organic
515 aerosol yields and composition from ozonolysis of monoterpenes at varying concentrations of NO₂, *Atmos.*
516 *Chem. Phys.*, 15(21), 12267–12281, doi:10.5194/acp-15-12267-2015, 2015.
- 517 Ehn, M., Kleist, E., Junninen, H., Petäjä, T., Lönn, G., Schobesberger, S., Dal Maso, M., Trimborn, A., Kul-
518 mala, M., Worsnop, D. R., Wahner, A., Wildt, J. and Mentel, T. F.: Gas phase formation of extremely oxi-
519 dized pinene reaction products in chamber and ambient air, *Atmos. Chem. Phys.*, 12(11), 5113–5127,
520 doi:10.5194/acp-12-5113-2012, 2012.
- 521 Ehn, M., Thornton, J. A., Kleist, E., Sipilä, M., Junninen, H., Pullinen, I., Springer, M., Rubach, F., Tillmann,
522 R., Lee, B., Lopez-Hilfiker, F., Andres, S., Acir, I. H., Rissanen, M., Jokinen, T., Schobesberger, S.,
523 Kangasluoma, J., Kontkanen, J., Nieminen, T., Kurtén, T., Nielsen, L. B., Jørgensen, S., Kjaergaard, H. G.,
524 Canagaratna, M., Maso, M. D., Berndt, T., Petäjä, T., Wahner, A., Kerminen, V. M., Kulmala, M., Worsnop,
525 D. R., Wildt, J. and Mentel, T. F.: A large source of low-volatility secondary organic aerosol, *Nature*,
526 506(7489), 476–479, doi:10.1038/nature13032, 2014.
- 527 Friedman, B. and Farmer, D. K.: SOA and gas phase organic acid yields from the sequential photooxidation
528 of seven monoterpenes, *Atmos. Environ.*, 187(January), 335–345, doi:10.1016/j.atmosenv.2018.06.003, 2018.
- 529 Fry, J. L., Kiendler-Scharr, A., Rollins, A. W., Brauers, T., Brown, S. S., Dorn, H. P., Dubé, W. P., Fuchs, H.,
530 Mensah, A., Rohrer, F., Tillmann, R., Wahner, A., Wooldridge, P. J. and Cohen, R. C.: SOA from limonene:
531 Role of NO₃ in its generation and degradation, *Atmos. Chem. Phys.*, 11(8), 3879–3894, doi:10.5194/acp-11-
532 3879-2011, 2011.
- 533 Glasius, M. and Goldstein, A. H.: Recent Discoveries and Future Challenges in Atmospheric Organic Chem-
534 istry, *Environ. Sci. Technol.*, 50(6), 2754–2764, doi:10.1021/acs.est.5b05105, 2016.
- 535 Griffin, R. J.: Organic aerosol formation from the oxidation of biogenic hydrocarbons, , 104(D3), 3555–3567,
536 1999.
- 537 Guenther, A., Baugh, B., Brasseur, G., Greenberg, J., Harley, P., Klinger, L., Serca, D., and Vierling, L.:
538 Isoprene emission estimates and uncertainties for the Central African EXPRESSO study domain, *J. Geophys.*
539 *Res. Atmos.*, 104(D23), 30625–30639, doi:10.1029/1999JD900391, 1999.
- 540 Guenther, A., Nicholas Hewitt, C., David, E., Fall, R., Chris, G., Tom, G., Peter, H., Klinger, L., Manuel, L.,
541 Mckay, W. A., Tom, P., Scholes, B., Steinbrecher, R., Tallamraju, R., Taylor, J. and Zimmerman, P.: A
542 global model of natural volatile organic compound emissions s Raja the balance Triangle changes in the
543 atmospheric accumulation rates of greenhouse Triangle Several inventories of natural and Exposure
544 Assessment global scales have been two classes Fores, *J. Geophys. Res.*, 100(94), 8873–8892,
545 doi:doi:10.1029/94JD02950, 1995.
- 546 Guenther, A., Geron, C., Pierce, T., Lamb, B., Harley, P. and Fall, R.: Natural emissions of non-methane
547 volatile organic compounds, carbon monoxide, and oxides of nitrogen from North America, *Atmos. Environ.*,
548 34(12–14), 2205–2230, doi:10.1016/S1352-2310(99)00465-3, 2000.
- 549 Hao, L. Q., Romakkaniemi, S., Yli-Pirilä, P., Joutsensaari, J., Kortelainen, A., Kroll, J. H., Miettinen, P.,
550 Vaattovaara, P., Tiitta, P., Jaatinen, A., Kajos, M. K., Holopainen, J. K., Heijari, J., Rinne, J., Kulmala, M.,
551 Worsnop, D. R., Smith, J. N. and Laaksonen, A.: Mass yields of secondary organic aerosols from the

- 552 oxidation of α -pinene and real plant emissions, *Atmos. Chem. Phys.*, 11(4), 1367–1378, doi:10.5194/acp-11-
553 1367-2011, 2011.
- 554 Henry, K. M., Lohaus, T. and Donahue, N. M.: Organic Aerosol Yields from α -Pinene Oxidation: Bridging
555 the Gap between First-Generation Yields and Aging Chemistry, *Environ. Sci. Technol.*, 46(22), 12347–
556 12354, doi:10.1021/es302060y, 2012.
- 557 Jacobson, M. Z.: Numerical techniques to solve condensational and dissolutional growth equations when
558 growth is coupled to reversible reactions, *Aerosol Sci. Technol.*, 27(4), 491–498,
559 doi:10.1080/02786829708965489, 1997.
- 560 Jenkin, M. E., Saunders, S. M. and Pilling, M. J.: The tropospheric degradation of volatile organic
561 compounds: A protocol for mechanism development, *Atmos. Environ.*, 31(1), 81–104, doi:10.1016/S1352-
562 2310(96)00105-7, 1997.
- 563 Jenkin, M. E., Young, J. C. and Rickard, A. R.: The MCM v3.3.1 degradation scheme for isoprene, *Atmos.*
564 *Chem. Phys.*, 15(20), 11433–11459, doi:10.5194/acp-15-11433-2015, 2015.
- 565 Jenkin, M. E., Wyche, K. P., Evans, C. J., Carr, T., Monks, P. S., Alfarra, M. R., Barley, M. H., McFiggans,
566 G. B., Young, J. C. and Rickard, A. R.: Development and chamber evaluation of the MCM v3.2 degradation
567 scheme for β -caryophyllene, *Atmos. Chem. Phys.*, 12(11), 5275–5308, doi:10.5194/acp-12-5275-2012, 2012.
- 568 **Jenkin, M. E., Valorso, R., Aumont, B., Rickard, A. R., Cnrs, U. M. R., Créteil, U. P. and Paris, U. De: Esti-**
569 **mation of rate coefficients and branching ratios for reactions of organic peroxy radicals for use in automated**
570 **mechanism construction, , (2), 7691–7717, 2019.**
- 571 Jokinen, T., Berndt, T., Makkonen, R., Kerminen, V.-M., Junninen, H., Paasonen, P., Stratmann, F.,
572 Herrmann, H., Guenther, A. B., Worsnop, D. R., Kulmala, M., Ehn, M. and Sipilä, M.: Production of
573 extremely low volatile organic compounds from biogenic emissions: Measured yields and atmospheric
574 implications, *Proc. Natl. Acad. Sci.*, 112(23), 7123–7128, doi:10.1073/pnas.1423977112, 2015.
- 575 Kanakidou, M., Seinfeld, J. H., Pandis, S. N., Barnes, I., Dentener, F. J., Facchini, M. C. and Dingenen, R.
576 Van: Organic aerosol and global climate modelling: a review, , 1053–1123, 2005.
- 577 Kang, E. and Root, M. J.: Introducing the concept of Potential Aerosol Mass (PAM), *Atmos. Chem. Phys.*,
578 (7), 5727–5744
- 579 Keywood, M. D., Varutbangkul, V., Bahreini, R., Flagan, R. C. and Seinfeld, J. H.: Secondary organic aerosol
580 formation from the ozonolysis of cycloalkenes and related compounds, *Environ. Sci. Technol.*, 38(15), 4157–
581 4164, doi:10.1021/es035363o, 2004.
- 582 Korhonen, H., Lehtinen, K. E. J. and Kulmala, M.: Atmospheric Chemistry and Physics Multicomponent
583 aerosol dynamics model UHMA: model development and validation, *Atmos. Chem. Phys.*, 4, 757–771,
584 doi:10.1002/erv.2305, 2004.
- 585 Kristensen, K., Cui, T., Zhang, H., Gold, A., Glasius, M. and Surratt, J. D.: Dimers in α -pinene secondary
586 organic aerosol: Effect of hydroxyl radical, ozone, relative humidity and aerosol acidity, *Atmos. Chem. Phys.*,
587 14(8), 4201–4218, doi:10.5194/acp-14-4201-2014, 2014.
- 588 Kristensen, K., Jensen, L. N., Glasius, M. and Bilde, M.: The effect of sub-zero temperature on the formation
589 and composition of secondary organic aerosol from ozonolysis of alpha-pinene, *Environ. Sci. Process.*
590 *Impacts*, 19(10), 1220–1234, doi:10.1039/c7em00231a, 2017.

- 591 Kroll, J. H., Ng, N. L., Murphy, S. M., Flagan, R. C. and Seinfeld, J. H.: Secondary organic aerosol formation
592 from isoprene photooxidation under high-NO_x conditions, *Geophys. Res. Lett.*, 32(18), 1–4,
593 doi:10.1029/2005GL023637, 2005.
- 594 Lambe, A. T., Onasch, T. B., Massoli, P., Croasdale, D. R., Wright, J. P., Ahern, A. T., Williams, L. R.,
595 Worsnop, D. R., Brune, W. H. and Davidovits, P.: Laboratory studies of the chemical composition and cloud
596 condensation nuclei (CCN) activity of secondary organic aerosol (SOA) and oxidized primary organic aerosol
597 (OPOA), *Atmos. Chem. Phys.*, 11(17), 8913–8928, doi:10.5194/acp-11-8913-2011, 2011.
- 598 Lambe, A. T., Chhabra, P. S., Onasch, T. B., Brune, W. H., Hunter, J. F., Kroll, J. H., Cummings, M. J.,
599 Brogan, J. F., Parmar, Y., Worsnop, D. R., Kolb, C. E. and Davidovits, P.: Effect of oxidant concentration,
600 exposure time, and seed particles on secondary organic aerosol chemical composition and yield, *Atmos.*
601 *Chem. Phys.*, 15(6), 3063–3075, doi:10.5194/acp-15-3063-2015, 2015.
- 602 Lee, A., Goldstein, A. H., Keywood, M. D., Gao, S., Varutbangkul, V., Bahreini, R., Ng, N. L., Flagan, R. C.
603 and Seinfeld, J. H.: Gas-phase products and secondary aerosol yields from the ozonolysis of ten different
604 terpenes, *J. Geophys. Res. Atmos.*, 111(7), 1–18, doi:10.1029/2005JD006437, 2006a.
- 605 Lee, A., Goldstein, A. H., Kroll, J. H., Ng, N. L., Varutbangkul, V., Flagan, R. C. and Seinfeld, J. H.: Gas-
606 phase products and secondary aerosol yields from the photooxidation of 16 different terpenes, *J. Geophys.*
607 *Res. Atmos.*, 111(17), 1–25, doi:10.1029/2006JD007050, 2006b.
- 608 Liu, J., D'Ambro, E. L., Lee, B. H., Lopez-Hilfiker, F. D., Zaveri, R. A., Rivera-Rios, J. C., Keutsch, F. N.,
609 Iyer, S., Kurten, T., Zhang, Z., Gold, A., Surratt, J. D., Shilling, J. E. and Thornton, J. A.: Efficient Isoprene
610 Secondary Organic Aerosol Formation from a Non-IEPOX Pathway, *Environ. Sci. Technol.*, 50(18), 9872–
611 9880, doi: 10.1021/acs.est.6b01872, 2016.
- 612 Miller, K. A., Siscovick, D. S., Sheppard, L., Shepherd, K., Sullivan, J. H., Anderson, G., L. and Kaufman J.
613 D.: Long-Term Exposure to Air Pollution and Incidence of Cardiovascular Events in Women, *N. Engl. J.*
614 *Med.*, 356(5), 447–458, doi:10.1002/anie.201206370, 2007.
- 615 Nannoolal, Y., Rarey, J. and Ramjugernath, D.: Estimation of pure component properties part 3. Estimation of
616 the vapor pressure of non-electrolyte organic compounds via group contribution and group interactions, *Fluid*
617 *Phase Equilib.*, 269(1–2), 117–133, doi: 10.1016/j.fluid.2008.04.020, 2008.
- 618 Nah, T., Sanchez, J., Boyd, C. M. and Ng, N. L.: Photochemical Aging of α -pinene and β -pinene Secondary
619 Organic Aerosol formed from Nitrate Radical Oxidation, *Environ. Sci. Technol.*, 50(1), 222–231,
620 doi:10.1021/acs.est.5b04594, 2016.
- 621 Ng, N. L. and Chhabra, P. S.: Effect of NO_x level on secondary organic aerosol (SOA) formation from the
622 photooxidation of terpenes, *Atmos. Chem. Phys.*, (7), 5159–5174, doi: 10.1016/j.cub.2015.10.018, 2007.
- 623 Öström, E., Putian, Z., Schurgers, G., Mishurov, M., Kivekäs, N., Lihavainen, H., Ehn, M., Rissanen, M. P.,
624 Kurtén, T., Boy, M., Swietlicki, E. and Roldin, P.: Modeling the role of highly oxidized multifunctional or-
625 ganic molecules for the growth of new particles over the boreal forest region, *Atmos. Chem. Phys.*, 17(14),
626 8887–8901, doi:10.5194/acp-17-8887-2017, 2017.
- 627 Pankow, J. F. and Asher, W. E.: SIMPOL.1: a simple group contribution method for predicting vapor
628 pressures and enthalpies of vaporization of multifunctional organic compounds, *Rev. Mex. Ciencias Farm.*,
629 (8), 2773–2796, doi:doi: 10.5194/acp-8-2773-2008, 2008.
- 630 Pathak, R., Donahue, N. M. and Pandis, S. N.: Ozonolysis of β -pinene: Temperature dependence of secondary
631 organic aerosol mass fraction, *Environ. Sci. Technol.*, 42(14), 5081–5086, doi:10.1021/es070721z, 2008.

- 632 Pathak, R. K., Stanier, C. O., Donahue, N. M. and Pandis, S. N.: Ozonolysis of α -pinene at atmospherically
633 relevant concentrations: Temperature dependence of aerosol mass fractions (yields), *J. Geophys. Res. Atmos.*,
634 112(3), 1–8, doi:10.1029/2006JD007436, 2007.
- 635 Presto, A. A., Huff Hartz, K. E. and Donahue, N. M.: Secondary organic aerosol production from terpene
636 ozonolysis. 2. Effect of NO_x concentration, *Environ. Sci. Technol.*, 39(18), 7046–7054,
637 doi:10.1021/es050400s, 2005.
- 638 Qi, X., Ding, A., Roldin, P., Xu, Z., Zhou, P., Sarnela, N., Nie, W., Huang, X., Rusanen, A., Ehn, M., Rissanen,
639 M. P., Petäjä, T., Kulmala, M. and Boy, M.: Modelling studies of HOMs and their contributions to new
640 particle formation and growth: Comparison of boreal forest in Finland and a polluted environment in China,
641 *Atmos. Chem. Phys.*, 18(16), 11779–11791, doi:10.5194/acp-18-11779-2018, 2018.
- 642 Quéléver, L. L. J., Kristensen, K., Jensen, L., Rosati, B., Teiwes, R., Daellenbach, K. R., Peräkylä, O., Roldin,
643 P., Pedersen, H. B., Glasius, M., Bilde, M. and Ehn, M.: Effect of temperature on the formation of Highly-
644 oxygenated Organic Molecules (HOM) from alpha-pinene ozonolysis, *Atmos. Chem. Phys.*, 1–29,
645 doi:10.5194/acp-2018-1276, 2019.
- 646 Roldin, P., Ehn, M., Kurtén, T., Olenius, T., Rissanen, M. P., Sarnela, N., Elm, J., Rantala, P., Hao, L., Hytti-
647 nen, N., Heikkinen, L., Worsnop, D. R., Pichelstorfer, L., Xavier, C., Clusius, P., Öström, E., Petäjä, T., Kul-
648 mala, M., Vehkamäki, H., Virtanen, A., Riipinen, I. and Boy, M.: The role of highly oxygenated organic mol-
649 ecules in the Boreal aerosol-cloud-climate system, *Nat. Commun.*, 10(1), 4370, doi:10.1038/s41467-019-
650 12338-8, 2019.
- 651 Rosenfeld, D., Andreae, M. O., Asmi, A., Chin M., De Leeuw, G., Donovan, D. P., Kahn, R., Kinne, S.,
652 Kivekäs, N., Kulmala, M., Lau W., Schmidt K, S., Suni T., Wagner T., Wild, M., and Quaas J., Global obser-
653 vations of aerosol-cloud-precipitation-climate interactions, *Rev. Geophys.*, 52, 750–808,
654 doi:10.1002/2013RG000441.
- 655 Rissanen, M. P., Kurtén, T., Sipilä, M., Thornton, J. A., Kausiala, O., Garmash, O., Kjaergaard, H. G., Petäjä,
656 T., Worsnop, D. R., Ehn, M. and Kulmala, M.: Effects of chemical complexity on the autoxidation
657 mechanisms of endocyclic alkene ozonolysis products: From methylcyclohexenes toward understanding α -
658 pinene, *J. Phys. Chem. A*, 119(19), 4633–4650, doi:10.1021/jp510966g, 2015.
- 659 Saathoff, H. and Naumann, K.-H.: Temperature dependence of yields of secondary organic aerosols from the
660 ozonolysis of α -pinene and limonene, *Atmos. Chem. Phys.*, (March), 4–15, doi:10.5194/acp-9-1551-2009,
661 2009.
- 662 Sarrafzadeh, M., Wildt, J., Pullinen, I., Springer, M., Kleist, E., Tillmann, R., Schmitt, S. H., Wu, C., Mentel,
663 T. F., Zhao, D., Hastie, D. R. and Kiendler-Scharr, A.: Impact of NO_x and OH on secondary organic aerosol
664 formation from β -pinene photooxidation, *Atmos. Chem. Phys.*, 16(17), 11237–11248, doi:10.5194/acp-16-
665 11237-2016, 2016.
- 666 Saunders, S. M., Jenkin, M. E., Derwent, R. G. and Pilling, M. J.: Protocol for the development of the Master
667 Chemical Mechanism, MCM v3 (Part A): Tropospheric degradation of non-aromatic volatile organic
668 compounds, *Atmos. Chem. Phys.*, 3(1), 161–180, doi:10.5194/acp-3-161-2003, 2003.
- 669 Schmale, J., Henning, S., Henzing, B., Keskinen, H., Sellegri, K., Ovadnevaite, J., Bougiatioti, A., Kalivitis,
670 N., Stavroulas, I., Jefferson, A., Park, M., Schlag, P., Kristensson, A., Iwamoto, Y., Pringle, K., Reddington,
671 C., Aalto, P., Äijälä, M., Baltensperger, U., Bialek, J., Birmili, W., Bukowiecki, N., Ehn, M., Fjærraa, A. M.,
672 Fiebig, M., Frank, G., Fröhlich, R., Frumau, A., Furuya, M., Hammer, E., Heikkinen, L., Herrmann, E.,

- 673 Holzinger, R., Hyono, H., Kanakidou, M., Kiendler-Scharr, A., Kinouchi, K., Kos, G., Kulmala, M.,
674 Mihalopoulos, N., Motos, G., Nenes, A., O'Dowd, C., Paramonov, M., Petäjä, T., Picard, D., Poulain, L.,
675 Prévôt, A. S. H., Slowik, J., Sonntag, A., Swietlicki, E., Svenningsson, B., Tsurumaru, H., Wiedensohler, A.,
676 Wittbom, C., Ogren, J. A., Matsuki, A., Yum, S. S., Myhre, C. L., Carslaw, K., Stratmann, F. and Gysel, M.:
677 Corrigendum: Collocated observations of cloud condensation nuclei, particle size distributions, and chemical
678 composition, *Sci. data*, 5, 180094, doi:10.1038/sdata.2018.94, 2018.
- 679 Shilling, J. E.: Particle mass yield in secondary organic aerosol formed by the dark ozonolysis of α -pinene,
680 *Atmos. Chem. Phys.*, 8(1992), 2073–2088, 2008.
- 681 Stirnweis, L., Marcolli, C., Dommen, J., Barmet, P., Frege, C., Platt, S. M., Bruns, E. A., Krapf, M., Slowik,
682 J. G., Wolf, R., Prévôt, A. S. H., Baltensperger, U. and El-Haddad, I.: Assessing the influence of NO_x con-
683 centrations and relative humidity on secondary organic aerosol yields from α -pinene photo-oxidation through
684 smog chamber experiments and modelling calculations, *Atmos. Chem. Phys.*, 17(8), 5035–5061, doi:10.5194/
685 acp-17-5035-2017, 2017.
- 686 Tasoglou, A. and Pandis, S. N.: Formation and chemical aging of secondary organic aerosol during the β -
687 caryophyllene oxidation, *Atmos. Chem. Phys.*, 15(11), 6035–6046, doi:10.519
- 688 Topping, D., Barley, M., Bane, M. K., Higham, N., Aumont, B., Dingle, N. and McFiggans, G.: UMan-
689 SysProp v1.0: an online and open-source facility for molecular property prediction and atmospheric aerosol
690 calculations, *Geosci. Model Dev.*, 9(2), 899–914, doi:10.5194/gmd-9-899-2016, 2016.
- 691 Waring, M. S.: Secondary organic aerosol formation by limonene ozonolysis: Parameterizing multi-
692 generational chemistry in ozone- and residence time-limited indoor environments, *Atmos. Environ.*, 144, 79–
693 86, doi:https://doi.org/10.1016/j.atmosenv.2016.08.051, 2016.
- 694 Zhao, D., Schmitt, S. H., Wang, M., Acir, I. H., Tillmann, R., Tan, Z., Novelli, A., Fuchs, H., Pullinen, I.,
695 Wegener, R., Rohrer, F., Wildt, J., Kiendler-Scharr, A., Wahner, A. and Mentel, T. F.: Effects of NO_x and
696 SO₂ on the secondary organic aerosol formation from photooxidation of α -pinene and limonene, *Atmos.*
697 *Chem. Phys.*, 18(3), 1611–1628, doi:10.5194/acp-18-1611-2018, 2018.
- 698 Zhao, D. F., Kaminski, M., Schlag, P., Fuchs, H., Acir, I. H., Bohn, B., Häsel, R., Kiendler-Scharr, A.,
699 Rohrer, F., Tillmann, R., Wang, M. J., Wegener, R., Wildt, J., Wahner, A. and Mentel, T. F.: Secondary
700 organic aerosol formation from hydroxyl radical oxidation and ozonolysis of monoterpenes, *Atmos. Chem.*
701 *Phys.*, 15(2), 991–1012, doi:10.5194/acp-15-991-2015, 2015.